C.1.

SOME NMR STUDIES OF $NbSe_2$

by

KHALED ABDOLALL
B.Sc., University of Waterloo, 1972

A THESIS SUBMITTED IN PARTIAL FULFILMENT OF
THE REQUIREMENTS FOR THE DEGREE OF
MASTER OF SCIENCE

in the Department
of
Physics

We accept this thesis as conforming to the
required standard

THE UNIVERSITY OF BRITISH COLUMBIA
April, 1974

In presenting this thesis in partial fulfilment of the requirements for an advanced degree at the University of British Columbia, I agree that the Library shall make it freely available for reference and study. I further agree that permission for extensive copying of this thesis for scholarly purposes may be granted by the Head of my Department or by his representatives. It is understood that copying or publication of this thesis for financial gain shall not be allowed without my written permission.

Department of PHYSICS

The University of British Columbia
Vancouver 8, Canada

Date APRIL 30/74

ABSTRACT

A sensitive nuclear magnetic resonance spectrometer has been constructed using Field Effect Transistors in a Robinson configuration. The spectrometer has been used to study the anomalous nuclear magnetic resonance spectra of single crystals of $NbSe_2$. An analysis of the field dependence of the line width in the low temperature phase has demonstrated that this results from a distribution of Knight Shifts. Such a distribution is not consistent with a structural transformation involving only two nonequivalent sites as proposed by Ehrenfreund et al. In addition accurate measurements of the Knight Shift and electric field gradient tensor have been made in the high temperature phase at 77K and 300K. The Knight Shift has a very large anisotropic component but an almost zero isotropic component which is indicative of negligible s-electron character at the Fermi surface.

TABLE OF CONTENTS

LIST OF TABLES

LIST OF ILLUSTRATIONS

ACKNOWLEDGEMENTS

I would like to express my sincere gratitude to Dr.D.L1. Williams for his valuable instruction throughout the work.

I would like to express my gratitude to Dr. M.I. Valic for his many valuable suggestions and his help in the experiments.

I am very grateful to Dr. Walter N. Hardy for his great help in explaining the circuit diagrams of the spectrometer, its theory of operation, and his valuable suggestions regarding its construction. I am also indebted to him for reviewing the section on the spectrometer.

CHAPTER I

INTRODUCTION

Niobium diselenide is a layered transition metal dichalcogenide which exists in three stacking polytypes. Wilson and Yoffe (1969) have published a thorough description of these layered structures and their properties. At room temperature the 2H polytype has a layered hexagonal structure that has the symmetry of the space group $P6_3/mmc$. This material showed an anomalous sign reversal of the Hall coefficient at 26K and a maximum in the magnetic susceptibility near 40K (Lee et al (1969)), which were taken to be indicative of a phase transformation.

NMR studies on powders of 2H-$NbSe_2$ were made by Ehrenfreund et al (1971). They conclude that the anomalous behaviour of $NbSe_2$ at low temperatures is due to a structural transformation and an associated conduction electron redistribution. In their model, they suggest that at and below 20K there are two inequivalent niobium sites with different electric field gradients. Their analysis is based on the information extracted from the powder pattern line shape, which is assumed to be the convolution of a Gaussian shape function with the frequency distribution expected from a randomly oriented microcrystalite sample in the presence of quadrupole effects and an inisotropic Knight shift.

The purpose of this work is to further study the properties of $NbSe_2$ by NMR methods using single crystals. The advantages of using single crystals (as was demonstrated in this laboratory in previous work on Gallium and Aluminium) are: (a) a direct study of the anisotropy in the Knight shift due to crystal symmetry, (b) elimination of line broadening caused by the anisotropic Knight shift, and (c) consequently more accurate measurements of the Knight shifts and the electric field gradient parameters.

CHAPTER II

THEORETICAL CONSIDERATIONS

The Quadrupolar Hamiltonian:

The Hamiltonian operator for the interaction of the nuclear quadrupole moment with the electric field gradient existing at the nucleus is given by [4]:

$$H_Q = \frac{e^2qQ}{4I(2I-1)} \left[3I_{Z'}^2 - I\,(I+1) + \frac{1}{2}\eta(I_+^2 + I_-^2)\right]$$

where

$$I_{\pm} = I_{X'} \pm iY_{Y'}; \quad I_{X'}, \quad I_{Y'} \text{ and } I_{Z'}$$

are the components of the nuclear spin I; eQ is the scalar quadrupole moment and η is an asymmetry parameter defined as:

$$\eta = \frac{q_{X'X'} - q_{Y'Y'}}{q_{Z'Z'}}$$

where

$$q_{X'X'}, \; q_{Y'Y'} \quad \text{and} \quad q_{Z'Z'} = q$$

are defined by the electric field gradient tensor;

$$\vec{\vec{q}} = \vec{\nabla}\vec{E} = \begin{pmatrix} -\frac{1}{2}(1-\eta)\,q_{X'X'} & 0 & 0 \\ 0 & -\frac{1}{2}(1+\eta)q_{Y'Y'} & 0 \\ 0 & 0 & q_{Z'Z'} \end{pmatrix}$$

and X', Y', Z' are the principal axes of $\vec{\vec{q}}$.

Energy levels in single crystals:

In the presence of an applied magnetic field $\vec{H}$ the Hamiltonian for a Spin I with a quadrupole moment is given by (Abragam P.232).

$$\underset{\sim}{H} = -\gamma h\vec{H}\cdot\vec{I} + \frac{eq^2Q}{4I\,(2\,I-1)}\left[3I_{Z'}^2 - I\,(I-1) + \frac{\eta}{2}\,(I_+^2 + I_-^2)\right]$$

(a) Crystals with cylindrical symmetry; magnetic field parallel to crystal axis.

For crystals with axial symmetry, which is the case of $NbSe_2$ at temperatures above 24 K, η vanishes because

$$q_{X'X'} = q_{Y'Y'}$$

If $\vec{H}$ is chosen parallel to the symmetry axis of the crystal (the Z' axis), then the Hamiltonian takes the form

$$\underset{\sim}{H} = - \gamma h H I_{Z'} + \frac{e^2qQ}{4I(2I-1)} [3I_{Z'}^2 - I\ (I+1)],$$

so that in the $|I, M_I>$ representation where $I_{Z'}$ is diagonal, the energies of the different levels are given by:

$$E_m = - \gamma h H m + \frac{e^2qQ}{4I(2I-1)} [3m^2 - I\ (I+1)]$$

or, using the notations

$$\nu_L = \frac{\gamma}{2\pi} H; \quad \nu_Q = \frac{3e^2qQ}{h2I(2I-1)}$$

The corresponding frequencies of the allowed transitions are

$$\nu_{m-1,m} = \frac{E_{m-1} - E_m}{h}$$

$$= \nu_L + \frac{\nu Q}{2} (1-2m)$$

For $I = \frac{9}{2}$ of the Nb^{93} nucleus the energy level diagram is given in Fig.(1).

Thus in a nuclear magnetic resonance experiment on Nb^{93} in $NbSe_2$ where the magnetic field is along the symmetry axis of the crystal one would expect to see nine lines corresponding to the frequencies:

$$\nu_r = \nu_L \pm r\nu_Q, \quad r = 0, 1, 2, 3, 4$$

with a central line corresponding to the $|\frac{9}{2}, \frac{1}{2}> \rightarrow |\frac{9}{2}, -\frac{1}{2}>$ transition and four satellites on each side equally spaced by ν_Q the quadrupole frequency of the Nb^{93} nucleus.

(b) Crystals with less than cylindrical symmetry; arbitrary orientations of the magnetic field.

For the more general problem of an arbitrary orientation of the magnetic field $\vec{H}$ the Hamiltonian takes the form

$$\underset{\sim}{H} = -\gamma h H \left\{\frac{\sin\theta\cos\phi}{2}(I_+ + I_-) - \frac{i\sin\theta\sin\phi}{2}(I_+ - I_-) + \cos\theta\, I_Z\right\}$$

$$+ \frac{e^2qQ}{4I(2I-1)}\left[3I_{Z'}^2 - I(I+1) + \frac{\eta}{2}(I_+^2 + I_-^2)\right]$$

where the angles θ, ϕ define the orientation of $\vec{H}$ with respect to the principal axes X', Y', Z' as shown in Fig. (2).

Making the substitution

$$\nu_L = \frac{\gamma}{2\pi}H,\quad \nu_Q = \frac{3e^2qQ}{h2I(2I-1)},\quad Y = \frac{6\nu_L}{\nu_Q}$$

gives

$$\underset{\sim}{H} = \frac{h\nu_Q}{6}\left[\left[-Y\left\{\frac{\sin\theta\cos\phi}{2}(I_+ + I_-) - \frac{i\sin\theta\sin\phi}{2}(I_+ - I_-) + \cos\theta\, I_{Z'}\right\}\right.\right.$$

$$\left.\left. + 3I_{Z'}^2 - I(I+1) + \frac{\eta}{2}(I_+^2 + I_-^2)\right]\right]$$

The appendix includes an explicit form of the 10 x 10 matrix of $\underset{\sim}{H}$ for a spin $I = \frac{9}{2}$ and a computer programme for diagonalizing such a matrix and finding the exact eigenvalues and the corresponding normalized eigenvectors.

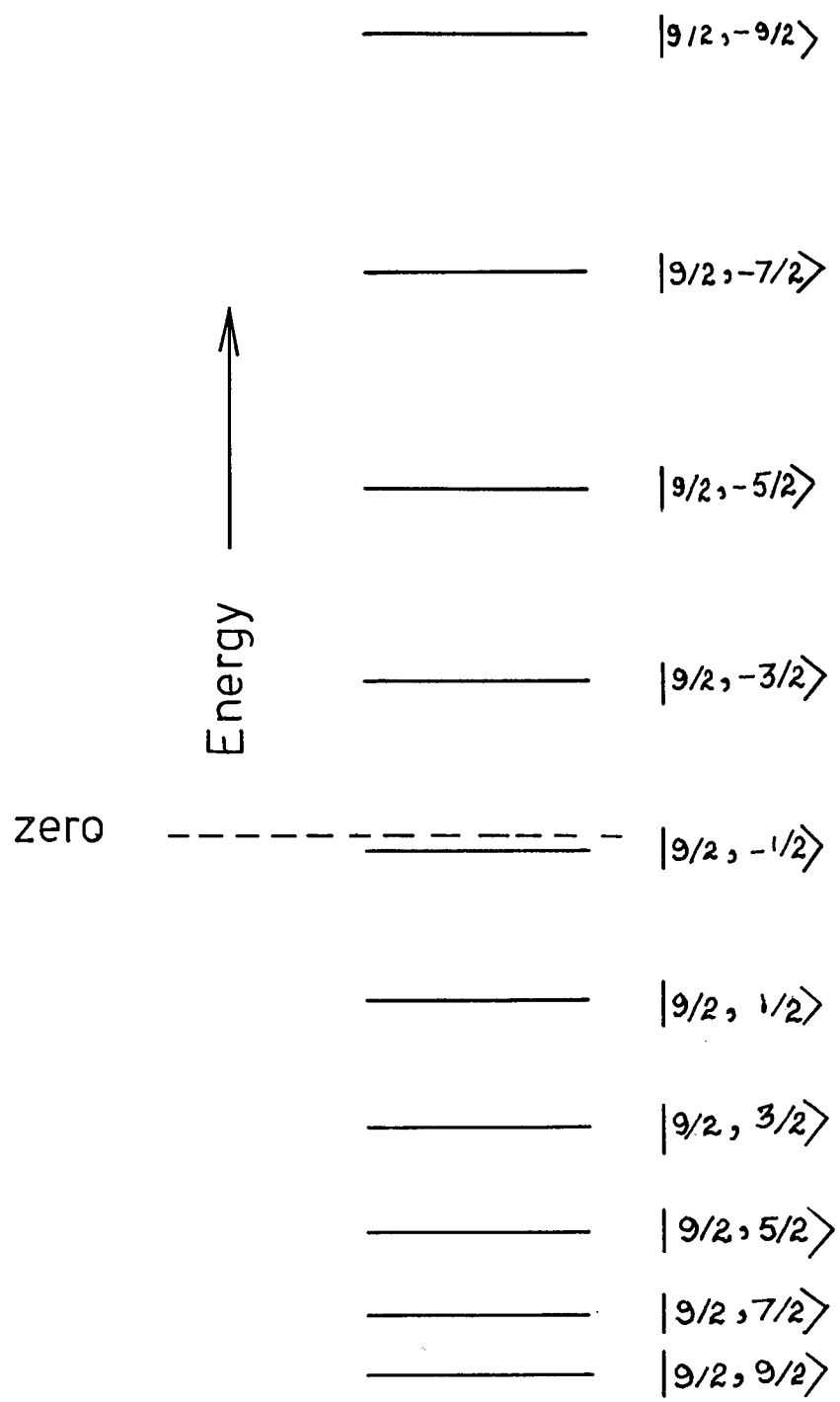

Fig. (1): Energy level diagrams for Nb^{93} nucleus of spin 9/2 in $NbSe_2$ single crystal with the magnetic field parallel to the high symmetry axis of the crystal (the c axis).

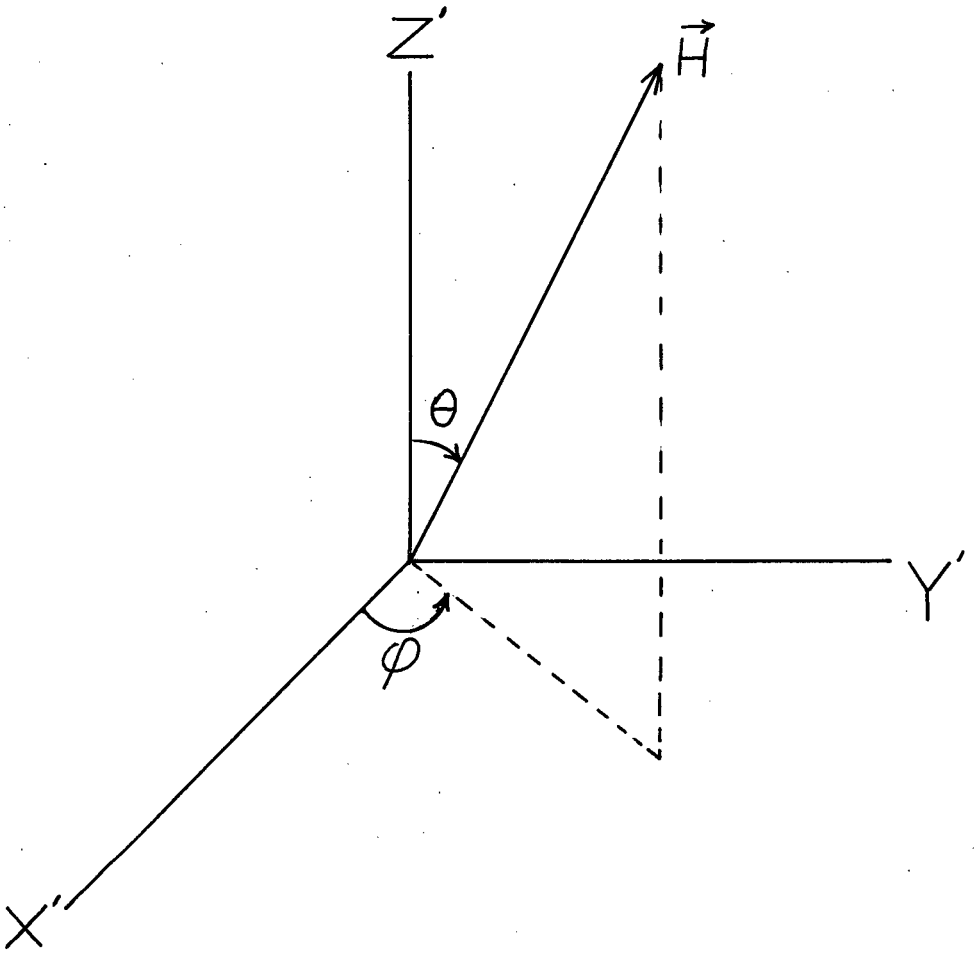

Fig. (2): Orientation of the magnetic field $\vec{H}$ with respect to the principal axes of the electric field gradient tensor.

THEORY OF THE KNIGHT SHIFT

For a given fixed applied field the nuclear magnetic resonance frequency for a nucleus in a metallic substance is different or 'shifted' from that of the same nucleus in a non metallic reference compound for the same applied field. This shift, known as the Knight Shift, is due to the interaction of the nuclear spins with the conduction electrons in the metal.

The Hamiltonian operator for the interaction of the conduction electrons with a nuclear spin I is given by [1];

$$\underset{\sim}{H}_{in} = 2\beta\gamma h \vec{I} \cdot \sum_{e} \{ \frac{\vec{\ell}}{r^3} - \frac{\vec{S}}{r^3} + \frac{3\vec{r}(\vec{S}.\vec{r})}{r^3} + \frac{8\pi}{3} \vec{S}\, \delta(\vec{r}) \} \tag{1}$$

where r and S are the position and spin of an electron e and ℓ is the orbital momentum. The summation is taken over all the electrons.

If the electronic orbital momentum is completely quenched then in the one electron description of the conduction electrons the expectation value of this operator is:

$$-\gamma h \vec{I} \cdot \sum_{k} \langle k | 2\beta \{ \frac{3(\vec{r}_k \cdot \vec{S}_k)\vec{r}_k}{r_k^5} - \frac{\vec{S}_k}{r_k^3} + \frac{8\pi}{3} \vec{S}_k \delta(\vec{r}) \} | k \rangle$$

$$= -\gamma h \vec{I} \cdot \sum_{k} \vec{\vec{\tau}}_k \cdot \vec{S}_k \tag{2}$$

where $\vec{\vec{\tau}}_k = \langle k | 2\beta \{ \frac{3\vec{r}_k \vec{r}_k}{r_k^5} - \frac{\vec{S}_k}{r_k^3} + \frac{8\pi}{3} \delta(\vec{r}_k) \} | k \rangle$

is a tensor with components depending on the states $|k\rangle$.

The summation is over unfilled states $|k\rangle$ because electrons in filled states do not contribute to this averaged interaction because their total spin moments are equal to zero.

If $\vec{\vec{\tau}}_k$ has approximately the same value for all unfilled states near the top of the Fermi distribution then

$$\gamma h \vec{I} \cdot \sum \vec{\vec{\tau}}_k \cdot \vec{S}_k = \gamma h \vec{I} \cdot \vec{\vec{\tau}} \cdot \vec{S} \qquad (3)$$

where

$$\vec{S} = \sum \vec{S}_k$$

If the tensors $\vec{\vec{\tau}}_k$ are not identical then $\vec{\vec{\tau}}$ is an average of $\vec{\vec{\tau}}_k$ over all the states $|k\rangle$ near the Fermi surface.

In the presence of an applied field H_o we have:

$$\vec{S} = - \frac{V}{2\beta} \chi \chi_p \vec{H}_o$$

where χ_p is the magnetic susceptibility per unit volume and it becomes a tensor if the orbital momentum is not completely quenched and V is the volume. Substituting for $\vec{S}$ in (3) gives

$$- \frac{V}{2\beta} \gamma h \vec{I} \cdot \chi_p \vec{\vec{\tau}} \cdot \vec{H}_o \qquad (4)$$

That is the nuclear spin $\vec{I}$ sees an additional field $V\chi_p \vec{\vec{\tau}} \cdot \vec{H}_o / 2\beta$ superimposed on $\vec{H}_o$ causing a shift in the nuclear resonance frequency.

In the one electron description the spatial correlation between the electrons is not taken into account. In fact it can be shown using the density matrix formalism [1] that relation (4) is independent of the one electron description.

Isotropic Knight Shift:

If the symmetry of the electronic environment of the nuclear spin is cubic or higher then only the scalar part of the tensor is different from zero, that is, only S electrons will contribute to the shift. In this case (4) reduces to

$$- V\gamma h \, (\vec{I} \cdot \vec{H}) \, \chi_p \cdot \frac{8\pi}{3} < | \psi(0) |^2 >_F$$

where $\psi(0)$ is the value of the wave function of an electron at the nucleus and the average $< >_F$ is made over all states at the top of the Fermi distribution. The total Hamiltonian becomes

$$-\gamma h \vec{I} \cdot \vec{H}_o \, (1 + V\chi_p \cdot \frac{8\pi}{3} < | \psi \, (0) |^2 >_F)$$

This corresponds to a positive frequency shift K given by

$$K_{iso} = \frac{\Delta H}{H_o} = \frac{8\pi}{3} V \chi_p < | \psi (0) |^2 >_F$$

Anisotropic Knight Shift

If the symmetry of the nuclear environment is less than cubic the tensor $\vec{\vec{\tau}}$ is not a scalar and the Knight shift will depend on the orientation of the applied magnetic field with respect to the crystal axis. Therefore we must add to the isotropic shift an anisotropic shift given by:

$$- \gamma h \vec{I} \cdot \vec{\vec{K}}' \vec{H}$$

$$= - \gamma h (I_{X'}, I_{Y'}, I_{Z'}) \begin{pmatrix} K'_{XX} & 0 & 0 \\ 0 & K'_{YY} & 0 \\ 0 & 0 & K'_{ZZ} \end{pmatrix} \begin{pmatrix} H_{X'} \\ H_{Y'} \\ H_{Z'} \end{pmatrix}$$

where $\vec{I}$, $\vec{\vec{K}}'$ and $\vec{H}$ are now defined with respect to the principal axes X', Y', Z' of the tensor $\vec{\vec{\tau}}$.

Since the anisotropic internal field is usually much smaller than the applied field H_o [9], the only effective component in shifting the resonance frequency is that along H_o which can be shown to be [1]

$$H_o (K'_{ZZ} \cos^2 \theta + K'_{XX} \sin^2 \theta \cos^2 \phi + K'_{YY} \sin^2 \theta \sin^2 \phi)$$

where θ, ϕ specify the orientation of H_o with respect to X',Y',Z'.

For axial symmetry we have

$$K'_{XX} = K'_{YY} = K'_{\perp}$$

$$K'_{ZZ} = - (K'_{XX} + K'_{YY}) \quad \text{from the traceless property of } \vec{\vec{K}}'$$

the relative frequency shift becomes

$$\frac{\Delta H}{H} = K_{iso} + \frac{1}{2} K'_{\parallel} (3 \cos^2 \theta - 1)$$

$$= K_{iso} + \frac{1}{2} K_{aniso} (3 \cos^2 \theta - 1)$$

where $K_{aniso} = K'_{\parallel}$ is a measure of the anisotropy in the charge distribution and is related to the conduction electron wave function by [6]

$$< \int |\psi_F|^2 \frac{(3 \cos^2 \theta - 1)}{r^3} d^3r >$$

which is a positive quantity if the charge density is greatest in the direction of the Z axis.

For the extreme cases we have

$$K_{\parallel} = K_{iso} + K_{aniso} \text{ for } \theta = 0$$

$$K_{\perp} = K_{iso} - \frac{1}{2} K_{aniso} \text{ for } \theta = \frac{\pi}{2}$$

This gives

$$K_{iso} = \frac{1}{3} (K_{\parallel} + 2 K_{\perp})$$

$$K_{aniso} = \frac{2}{3} (K_{\parallel} - K_{\perp})$$

CHAPTER III

EXPERIMENTAL

A brief introduction to steady state detection of NMR:

Steady state detection of nuclear magnetic resonance absorption consists of observing the response of the nuclear spin system to a continuously applied radio frequency field. The specimen is placed inside an r.f. coil which forms part of a tuned circuit as shown in Fig. (3). At resonance the nuclear spin system absorbs energy from the r.f. field H_1 inside the coil. This resonance effect is detected by its reaction on the circuit supplying the r.f. field.

The nuclear resonance absorption by the spins within the coil changes the quality factor, Q, of the coil by [5]:

$$\delta \left(\frac{1}{Q}\right) = 4 \pi \eta \chi''$$

where

η is the filling factor and χ'' is the imaginary part of the nuclear susceptibility.

If in the absence of signal the r.f. voltage across the coil is V_1 then near resonance a change by $\delta \left(\frac{1}{Q}\right)$ will result in

$$\delta V_1 = V_1 Q \delta \left(\frac{1}{Q}\right)$$

Thus detection of nuclear magnetic resonance absorption is reduced to detecting the change in the r.f. level across the coil containing the sample.

A variety of circuits for detecting nuclear magnetic resonance absorption have been used. The two most successful of the single coil types are the one by Robinson [5], and the one by Pound, Knight and Watkins [8].

APPARATUS

1: The Spectrometer:

For this work a transistorized version of the Robinson circuit using Field Effect Transistor (FETS) was built. The circuit was designed by Professor V. Frank

at the Technical University of Denmark. The following is a description of such a circuit, its principle of operation, construction design and an evaluation of its performance.

I. a) The r.f. Amplifier:

The r.f. amplifier is wide band and consists of an input stage and four amplifier stages that are connected in cascade with the input stage. Fig. (4) is the circuit diagram.

The FETS Q_1, Q_2, Q_3 and Q_4 form two cascodes in parallel. A cascode amplifier configuration is obtained using a common source and a common gate FET connected as shown in Fig. (5).

This configuration offers good stability, low noise amplification, and large power gain.

The stability is due to the reduced Miller effect in the common source stage and the small drain source capacitance of the common gate stage. Both factors contribute to a very small reverse transfer admittance for the combination.

Its low noise amplification is due to the fact that the voltage gain of the first stage is unity and therefore does not contribute to the noise. While the second stage allows amplification without addition in noise [3]. Thus the noise figure of the combination corresponds to the noise figure of the first stage.

The large power gain of the cascode is a result of the decreased output admittance.

The parallel combination of the two cascodes reduces the noise voltage of the input stage by a factor of two, giving further improvement in low noise amplification when the source impedance is less than the optimum value.

Q_5 and Q_6 are in the emitter follower configuration. The parallel arrangement provides low output impedance.

The remaining four amplifier stages each consist of a common source configuration followed by an emitter follower configuration. The emitter follower serves as a power amplifier as well as an impedance matching device.

The total voltage gain of the r.f. amplifier can be varied in steps from 4.6 to 1430.

I. b) Noise figure of the r.f. amplifier:

The noise figure of the r.f. amplifier was measured for different values of source impedance at a frequency of 10 MHz. The results are shown in Table (I) below.

SOURCE IMPEDANCE	NOISE FIGURE
244 Ω	3.44
.984 K	1.44
7.3 K	1.46

Table (I): Noise figure of the r.f. amplifier for 3 different source impedances.

II: The Limiter:

The circuit is shown in Fig. (6). The source follower Q_9 makes use of the high dynamic resistance in the source circuit provided by the constant current supply Q_{10}. This improves the linearity and performance of the source follower.

The input signal for the limiter is the output of the r.f. amplifier. The output of the source follower is applied to a pair of diodes D_1 and D_2 called 'clippers'. The output waveform is limited to the voltages set by the reverse biases of D_1 and D_2. Diodes D_3, D_4, D_5 and D_6 provide the necessary bias voltages. The limiting action can be adjusted by altering the reverse

bias voltages of D_1 and D_2 by means of the switching arrangement shown.

The arrangement of Q_{11} and Q_{12} forms a source coupled 0°/180° phase inverter. Since each amplifier stage changes the phase by 180°, the phase inverter is necessary to ensure that the total phase shift is zero when the number of amplifier stages is odd.

III: The Detector:

Detection is the process of recovering from a modulated r.f. carrier a signal that varies in accordance with the modulation present on the carrier.

Several methods of detection are available. The method used in this spectrometer makes use of the non-linear relation (approximately quadratic) between the gate bias and drain current of a FET.

Fig. (7) is a circuit diagram of the detector. Q_{13} is biased nearly to pinch off and therefore is operating in the non-linear region. When a modulated r.f. carrier is applied to the gate the averaged output signal will vary approximately as the modulation envelope. This is illustrated in Fig. (8).

The D.C. component of the rectified signal is amplified by the D.C. amplifier Q_{14}. The r.f. level is then monitored using a D.C. ammeter. The variable resistance R_o serves as a D.C. off-set for the D.C. amplifier.

IV: The Audio Amplifier:

The output of the detector is amplified by the low noise audio amplifier shown in Fig. (9). The low frequency components of the detector output are blocked by the high pass filter at the input of the amplifier. Q_{15} and Q_{16} are in common source configuration and Q_{17} is in a source follower configuration. The three stages are connected in cascade and a gain of about 3200 is achieved. The frequency response is shown in Fig. (10).

The high frequency rolloff of the amplifier is at 1.1 kHz. A higher frequency rolloff at 12 kHz can be obtained by means of the 5 nF capacitor shown in the diagram.

V: Principle of Operation:

A block diagram of the spectrometer is shown in Fig. (12).

Oscillations in the tank circuit are sustained by the positive feed-back provided by the limiter through the attenuator. If the phase shift between the input of the r.f. amplifier and the output of the attenuator (as the r.f. signal goes through the r.f. amplifier , limiter, and attenuator) is precisely zero, oscillations will occur at the centre of the resonance curve of the tuned circuit. Under such conditions the oscillation amplitude is least sensitive to small changes in frequency.

However, if phase shifts are introduced by some elements of the circuit such as stray capacitances, etc. oscillations will still occur, but in order to maintain a zero phase shift, the frequency of oscillation will be shifted from the centre of the resonance curve. In this case a small change in frequency can cause a large change in oscillation amplitude and the spectrometer will not be operating under optimum conditions. This is illustrated in Fig. (13).

The r.f. level across the coil is determined by the amount of feed-back. Lower r.f. levels are obtained by decreasing the amount of feed-back and adjusting the gain of the r.f. amplifier such that its output is sufficient to drive the limiter.

Nuclear resonance absorption changes the quality factor of the coil and thus changes the r.f. level across it. In the presence of an audiomodulated magnetic field the spin system will go in and out of resonance periodically with a frequency equal to that of the modulation frequency. Consequently the r.f. level across the coil will be amplitude modulated. This is amplified by the r.f. amplifier and then fed into the detector. The output of the detector is

approximately proportional to the modulation envelope and is further amplified by the audio stage. The output is then either displayed on a scope or, in the case of weak signals, is fed into a phase sensitive detector to improve the signal to noise ratio. By the nature of phase sensitive detection one obtains the derivative of the absorption signal rather than the signal itself.

VI: Construction Design of the Spectrometer:

Fig. (14) is a layout of the spectrometer. Each stage is enclosed in a separate compartment to shield it from other stages and outside interference. The r.f. amplifier stages, limiter and attenuator are arranged in the way shown to eliminate the undesirable use of a coaxial line in the feedback loop.

Feed through capacitors were used to provide the supply voltage as well as rigid supports for mounting the FET's. Ground lugs were soldered directly to the chassis. Whenever it was practical only one ground point was used for each stage. This has the effect of reducing self oscillations and ground loops. The leads were kept as short as possible in order to reduce stray pick up and microphonics.

Double pole double throw switches JMT 223 were used for connecting r.f. amplifier stages in cascade. In one position of the switch the amplifier stage is connected, in the other it is bypassed.

In the limiter a double pole five position rotary switch Alcoswitch MRA-25 is used. It provides 5 limiting options.

All the sides of the spectrometer were made removable except the front panel where all the control knobs are mounted. This provides easy access to all the components.

VII: Performance:

The circuit performed with good sensitivity throughout the frequency range 4 - 40 MHz. Typical absorption spectra are shown in Figs. (20), (21), and (22). No attempt was made to compare the sensitivity of this circuit with that of the marginal oscillator (Pound Knight box) presently used in this lab. However, according to Professor V. Frank the circuit is capable of performing with a sensitivity about a factor of 2 better than that of the marginal oscillator.

Additional advantages of this circuit over the marginal oscillator circuit are [5],(a) it can be adjusted to very low r.f. levels; (b) it can be used with circuits of very low L/C ratio. If the shunt impedance of the tuned circuit is low, not only is the noise figure of a marginal oscillator impaired, but also the circuit may fail to oscillate at all.

In the case of a metal sample the coil can be wound directly on the sample when using a Robinson circuit. But for the marginal oscillator it is often necessary to wrap a piece of mylar around the sample before winding the coil in order for the circuit to oscillate. This reduces the filling factor and thus affects the sensitivity. In conclusion this makes the Robinson circuit more attractive for NMR studies of metal single crystals.

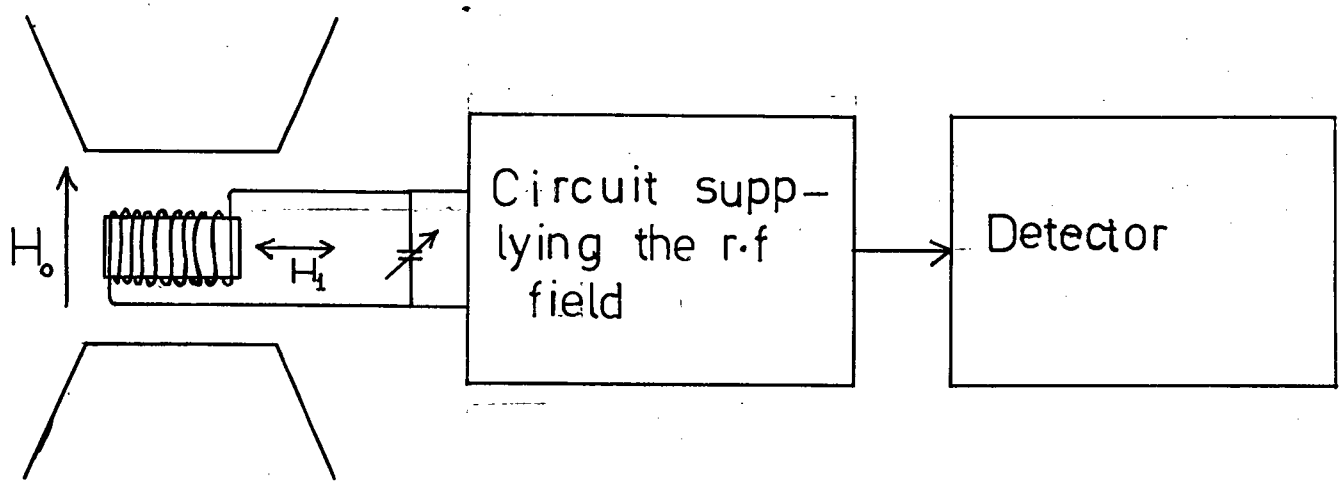

Fig. (3): Schematic arrangement for steady state NMR absorption experiments.

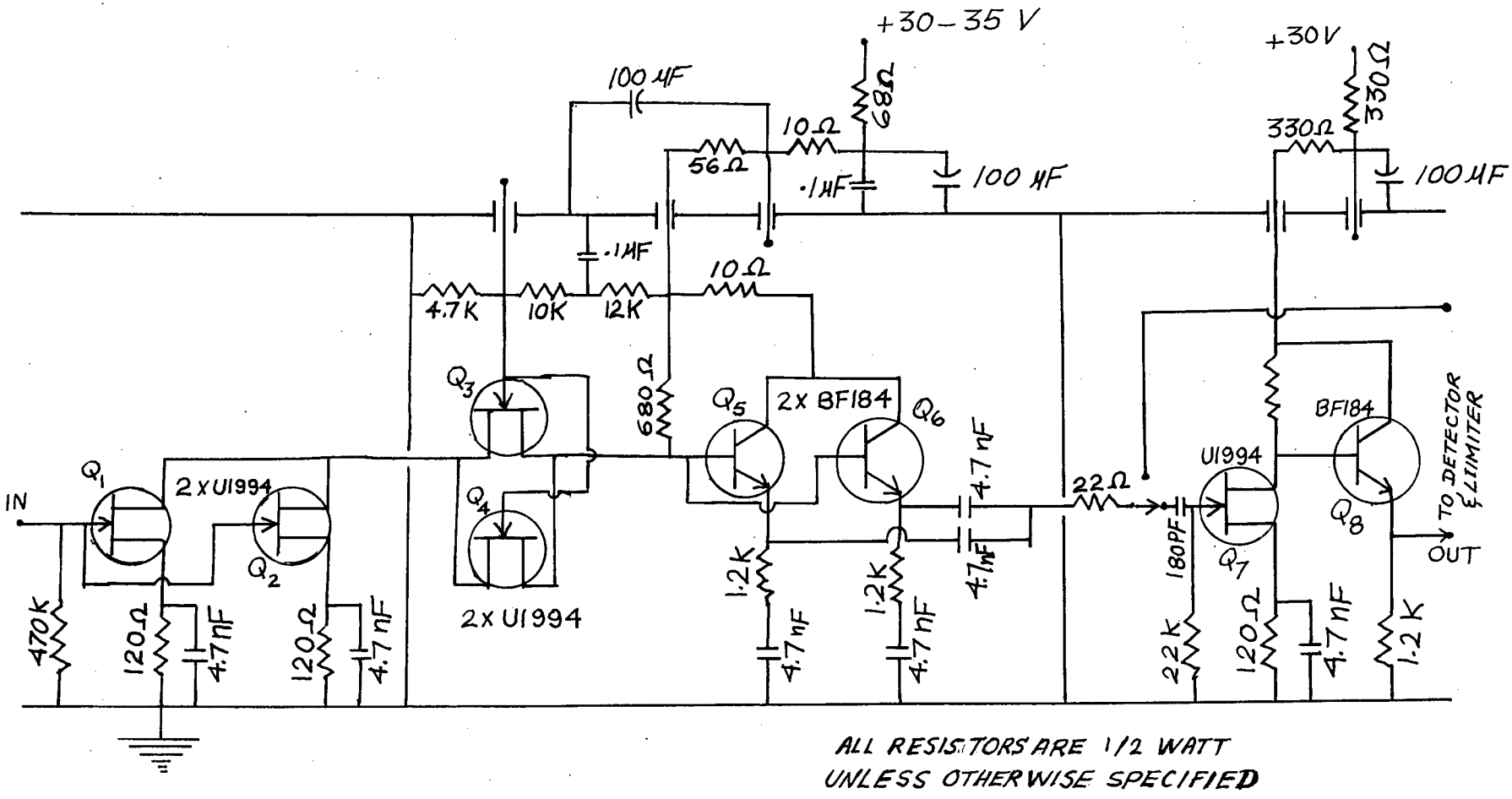

Fig. (4): The r.f. amplifier

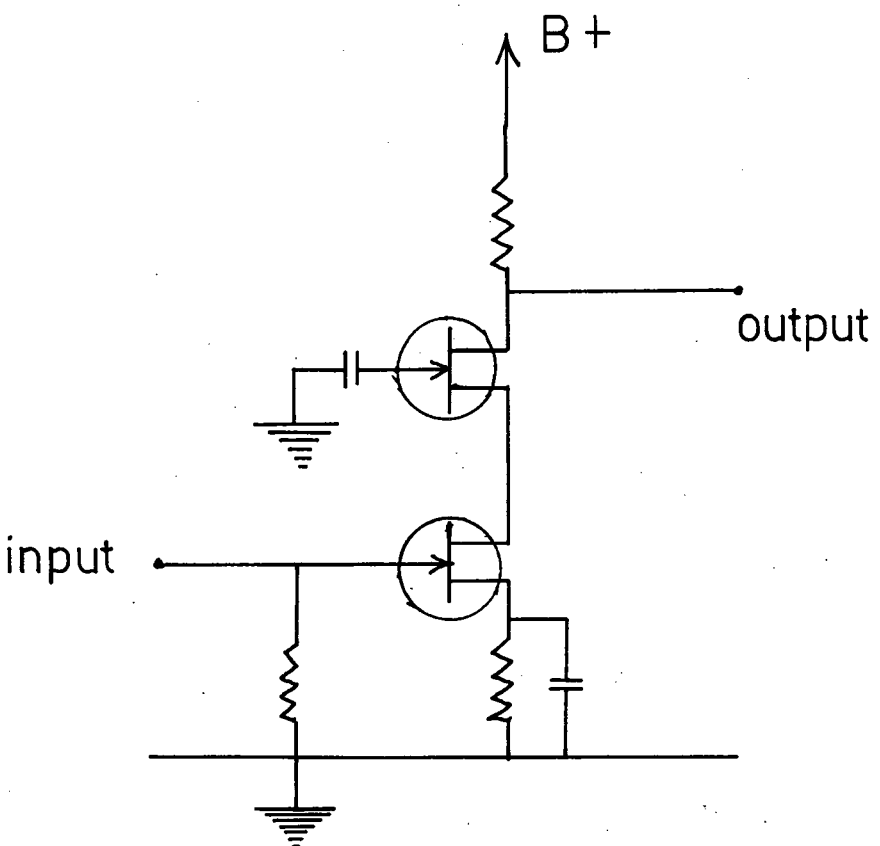

Fig. (5): A cascode amplifier

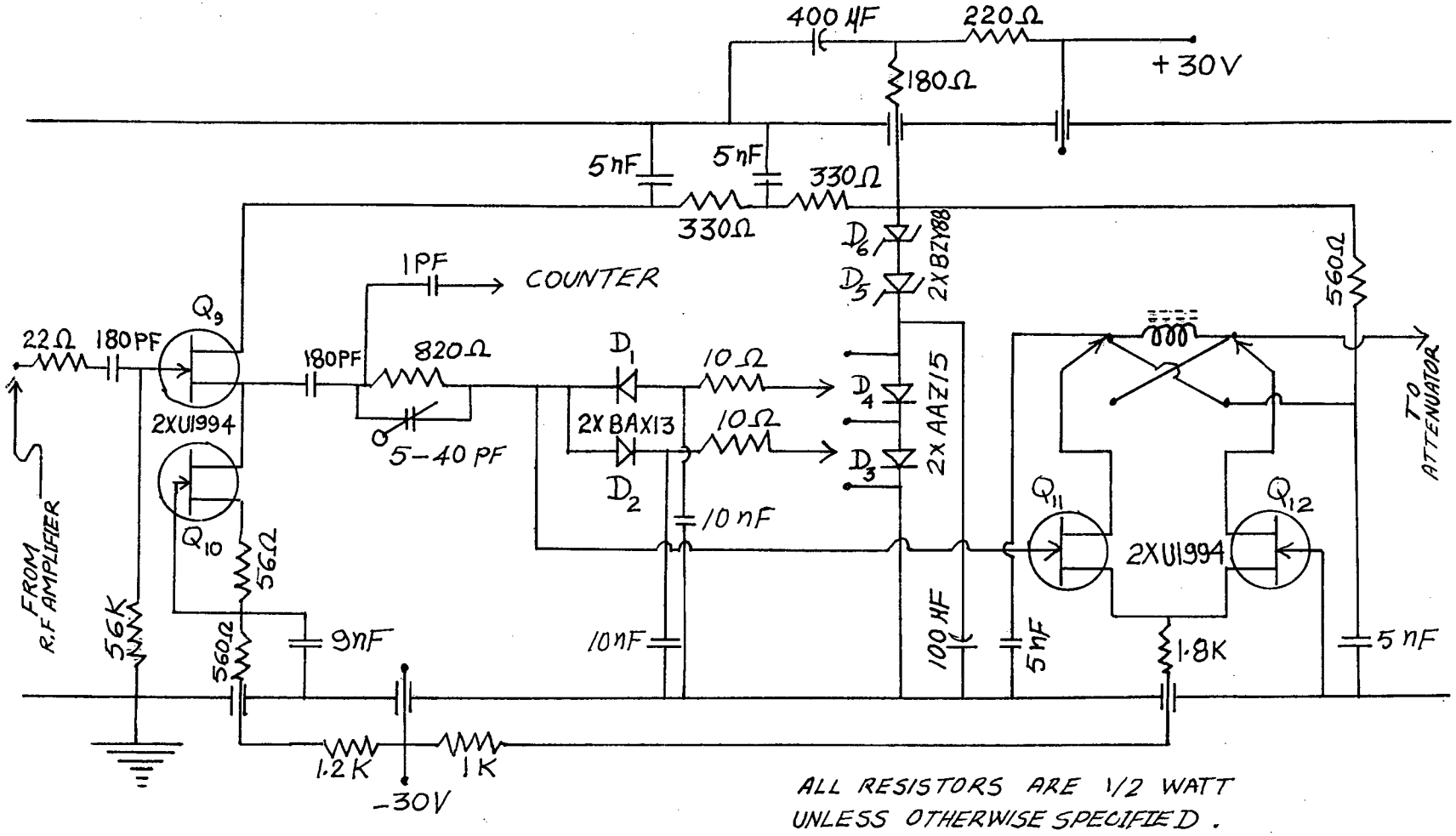

Fig. (6): The limiter

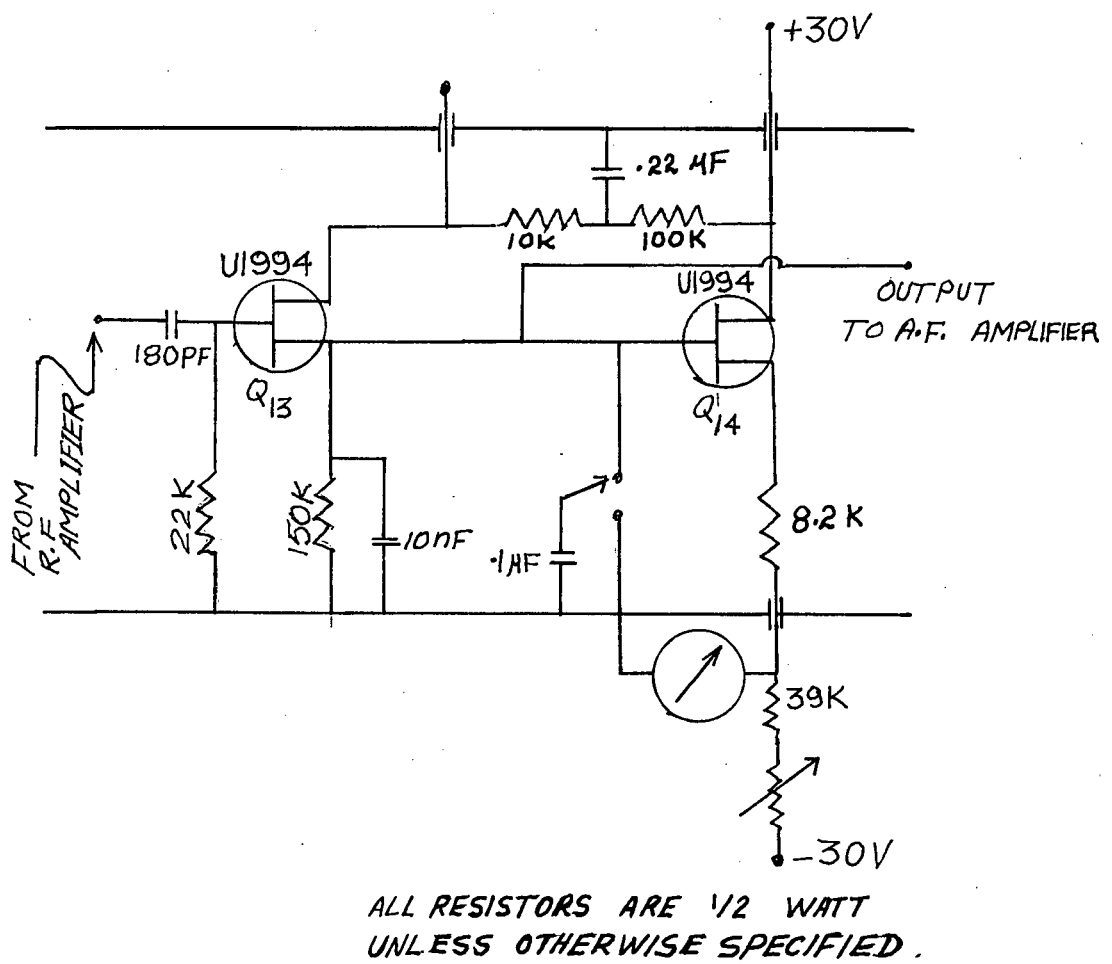

Fig. (7): The detector

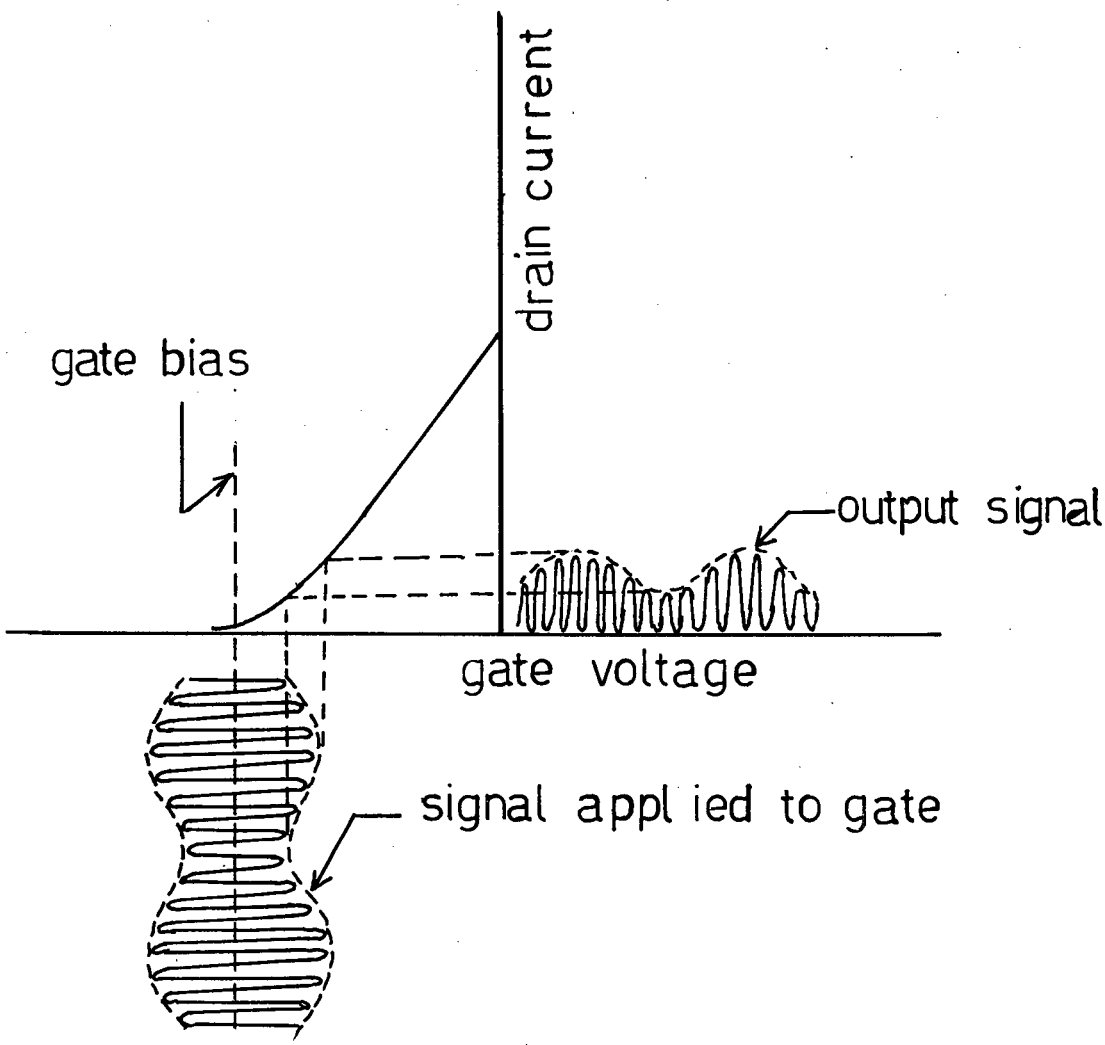

Fig. (8): Schematic diagrams of the detection process using the nonlinear relation between the gate bias and drain current of a FET.

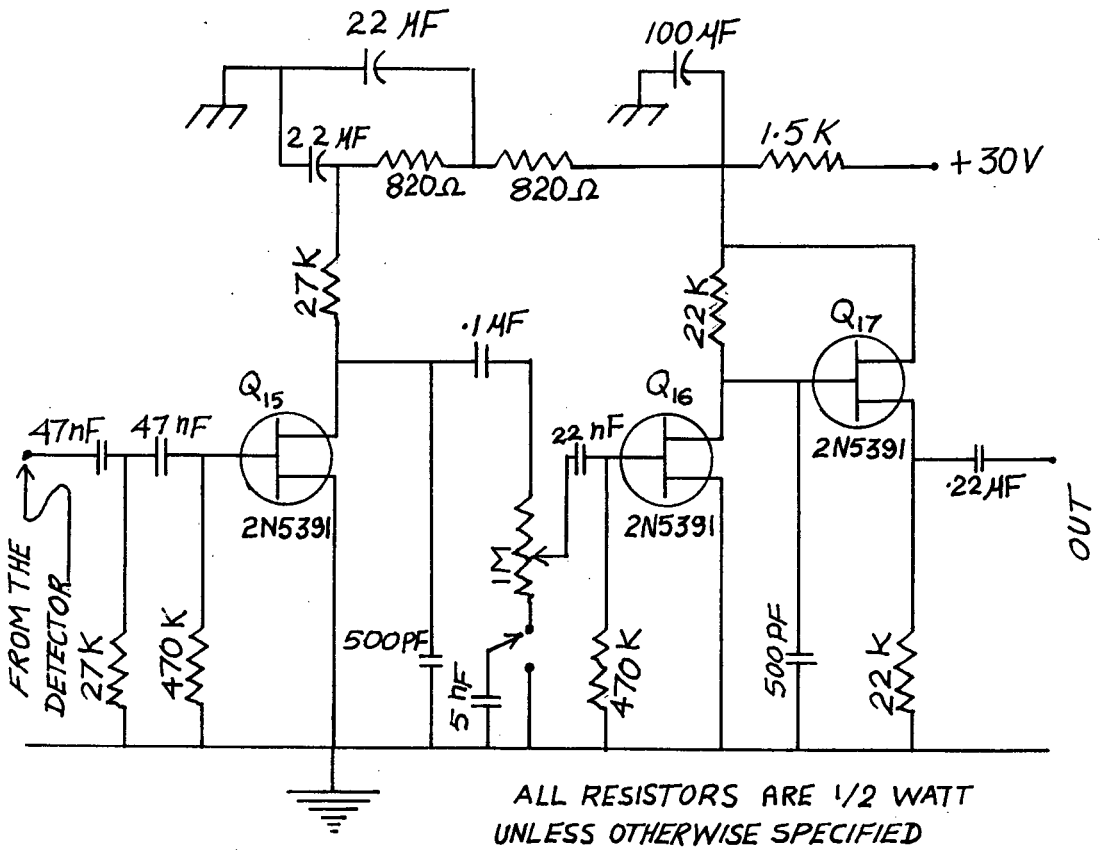

Fig. (9): The Audio Amplifier

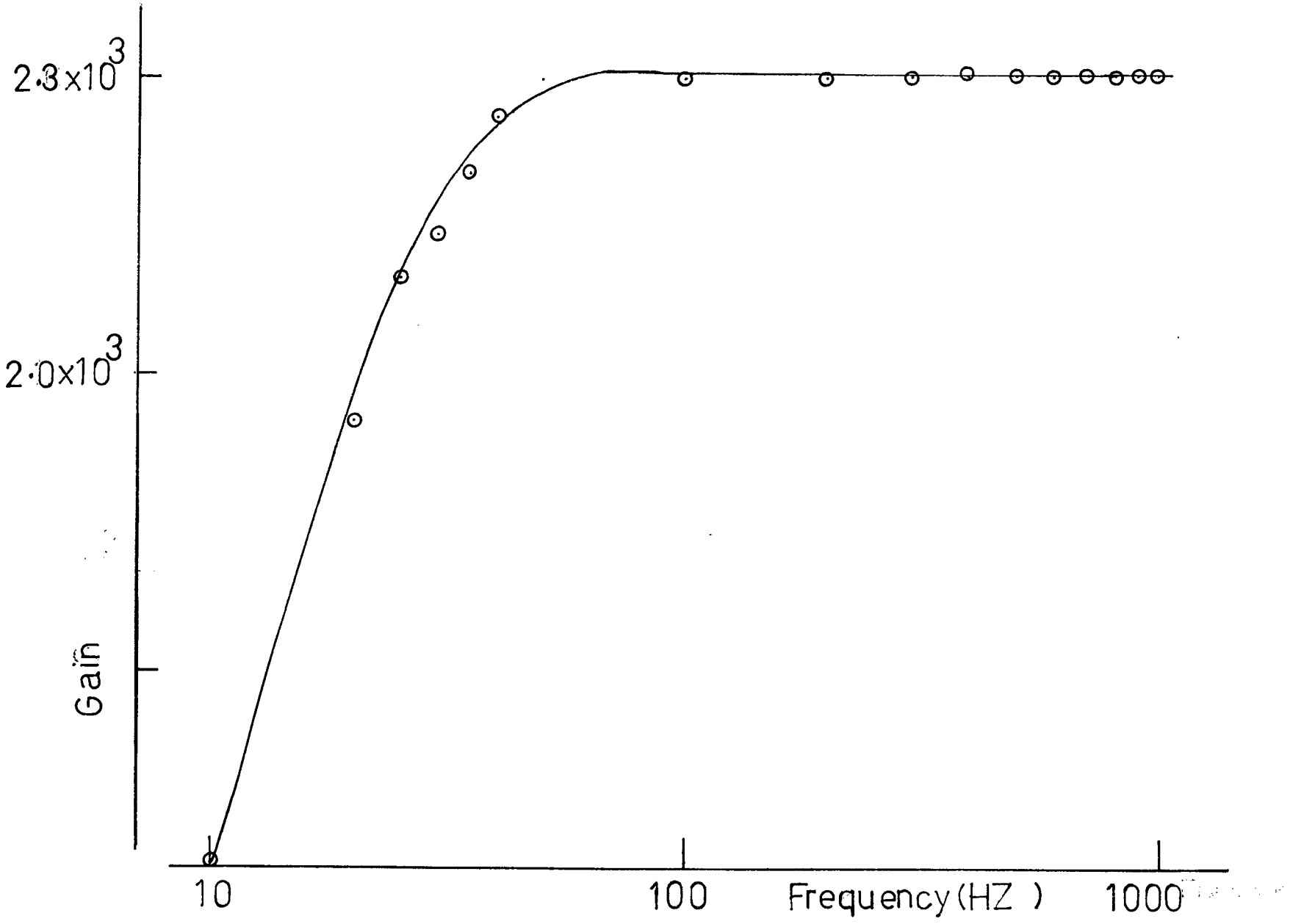

Fig. (10): Frequency response of the audio amplifier

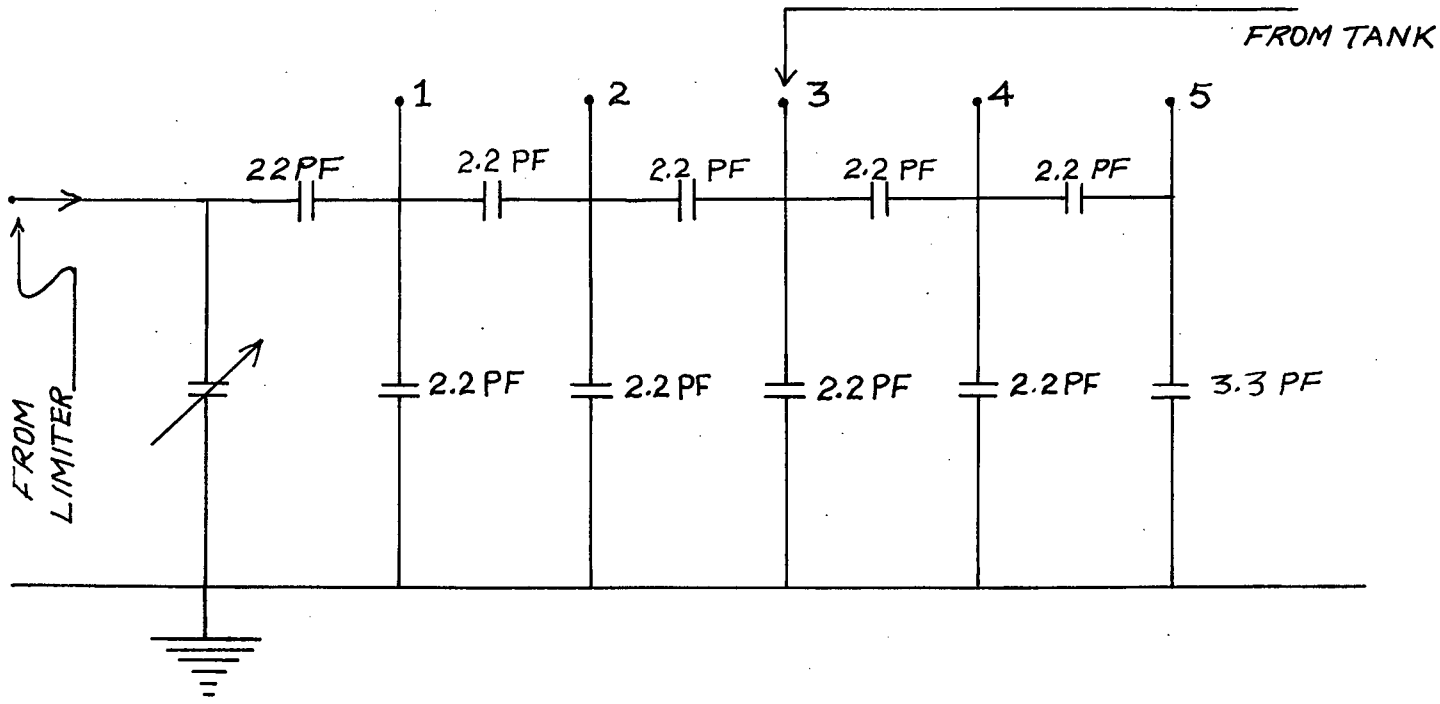

Fig. (11): The Attenuator

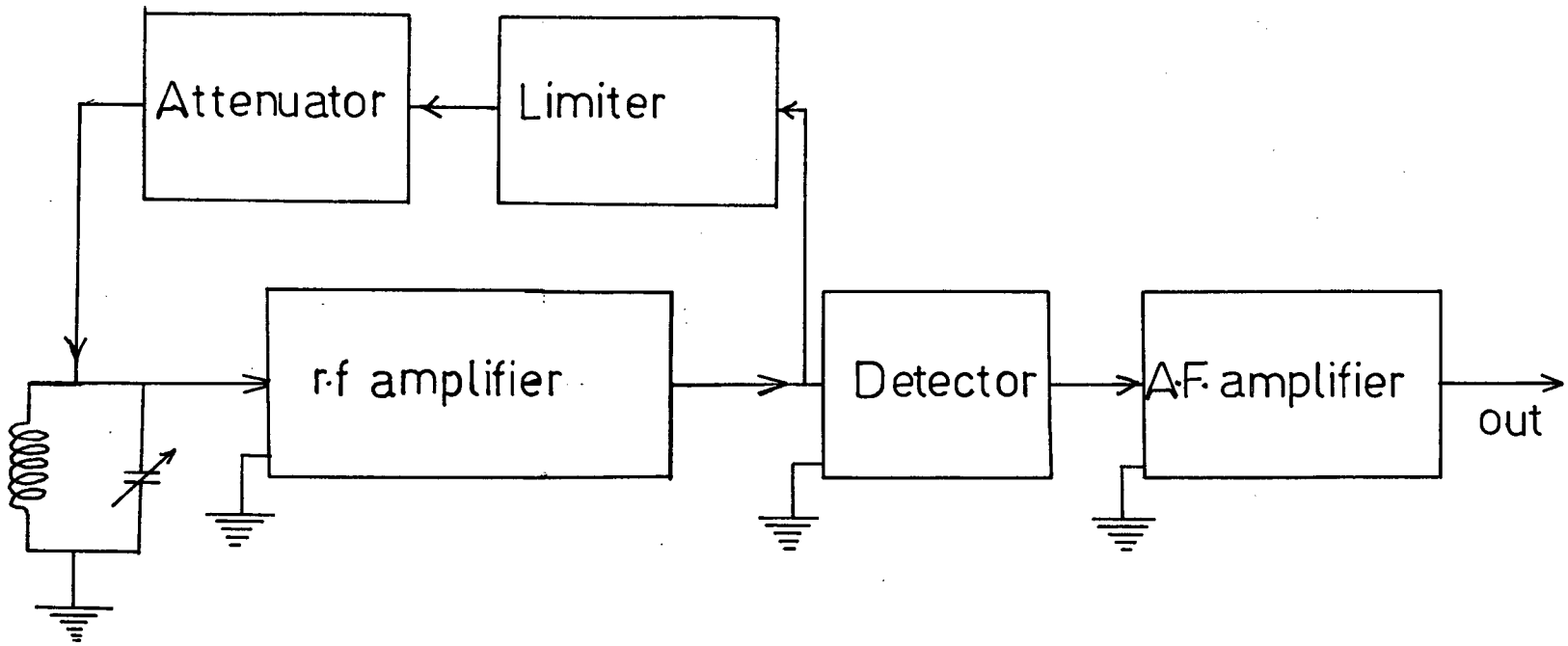

Fig. (12): A block diagram of the spectrometer

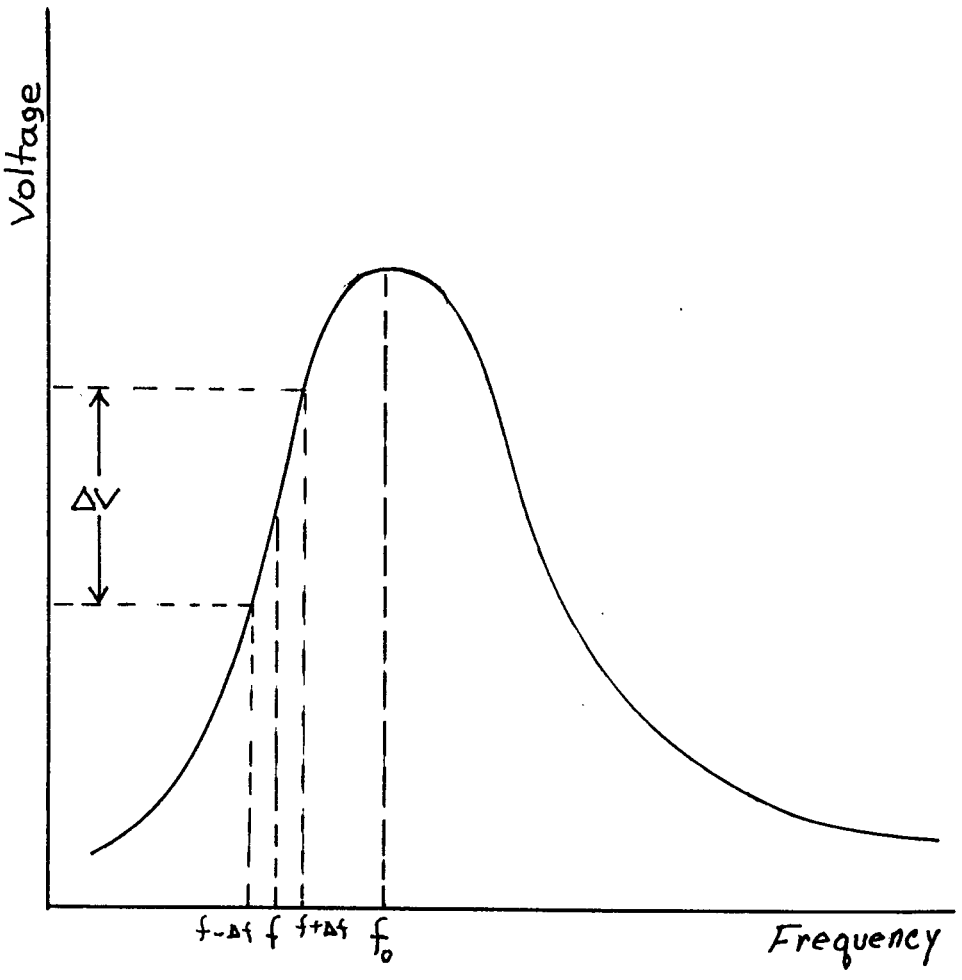

Fig. (13): Resonance curve of a tuned LC Circuit. It shows how a noise voltage ΔV is introduced by a small change $\mp\Delta f$ where f is the oscillation frequency different from that of the resonance frequency f_o of the tank.

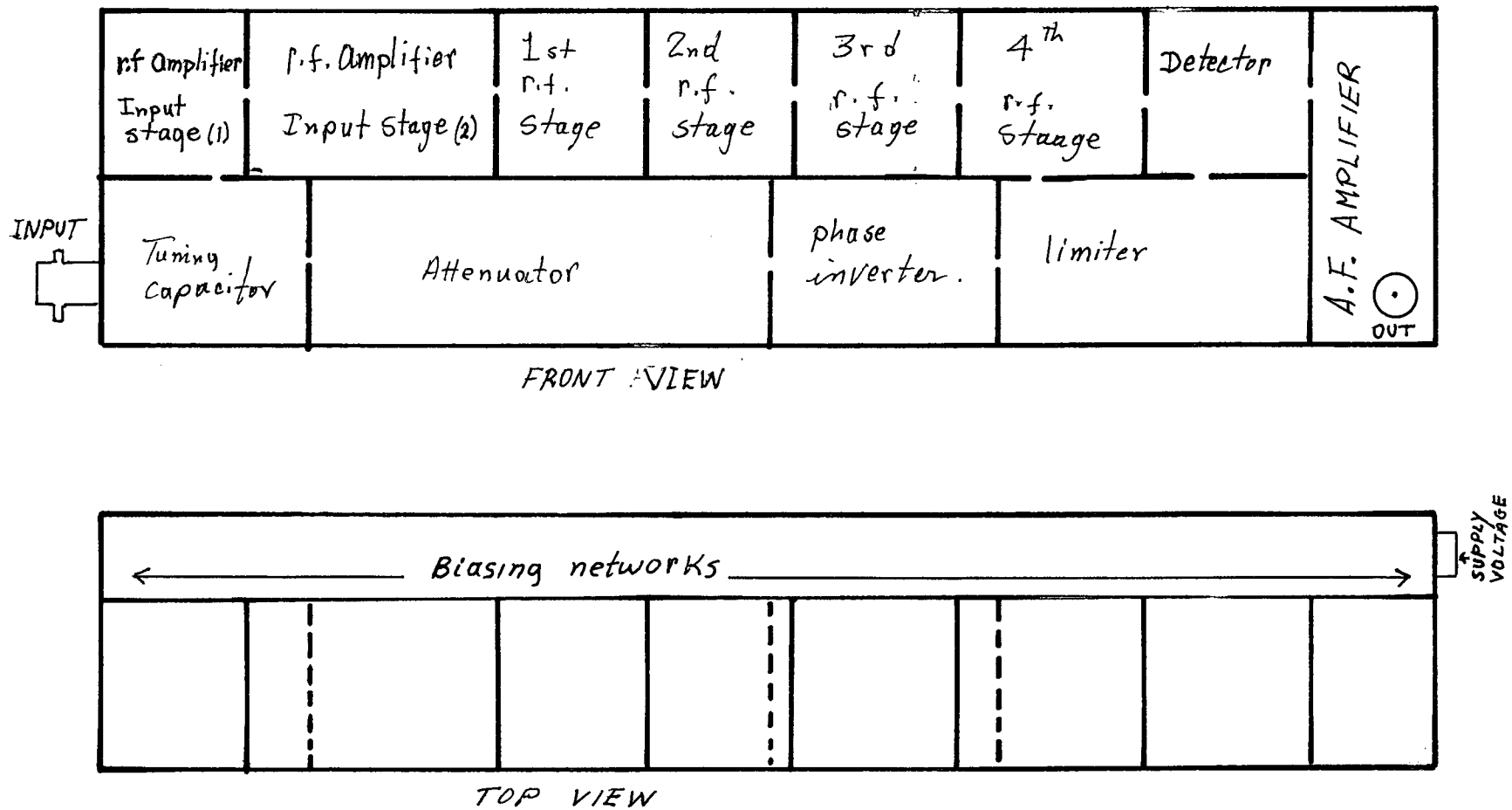

Fig. (14): Construction layout of the spectrometer

2. Sample and Crystal Holder:

A single crystal of $NbSe_2$ was obtained from Dr. R. Frindt of Simon Fraser University, grown in the form of a thin sheet (about .1 mm thick) with the c axis perpendicular to the plane of the sheet.

To minimize damage to the crystal, the sample was placed between two thin sheets of mylar before the r.f. coil of #40 copper wire was wound on it. The whole sample assembly was glued with varnish onto a thin microscope slide which was then glued to the copper block as shown in Fig. (15).

3. Orientation of the Crystal:

Initial orientation of the crystal c-axis was done visually. The final orientation was then determined from the angular dependence of the $|\frac{9}{2} - \frac{1}{2}> \rightarrow |\frac{9}{2} - \frac{1}{2}>$ resonance. By rotating the magnet and finding the resonance field the graph of Fig. (16) was obtained. From this graph the orientation of the c axis was determined to within half a degree.

4. Temperature Control:

Regulation of temperature between 4.2 K and 50 K is achieved by electrical heating in the low temperature cryostat, shown in Fig. (15).

Desired temperatures were obtained by a manual control of the heating current and the amount of exchange gas inside the cryostat. For temperatures above 20°K it was necessary to pump out all the exchange gas in order to reduce the heater current and thus minimize Helium boil-off. As a result the time required for the Cu block and sample to reach thermal equilibirum was much longer (about 30 minutes).

For measuring the temperature a gold + .03% at Fe Vs chromel thermocouple was used. The reference junction was kept at 4.2 K by ensuring that it was in contact with the brass block at the bottom of the cryostat which was in turn in direct contact with the helium bath. The thermocouple voltage was measured with a Keithley 148 nanovolt meter.

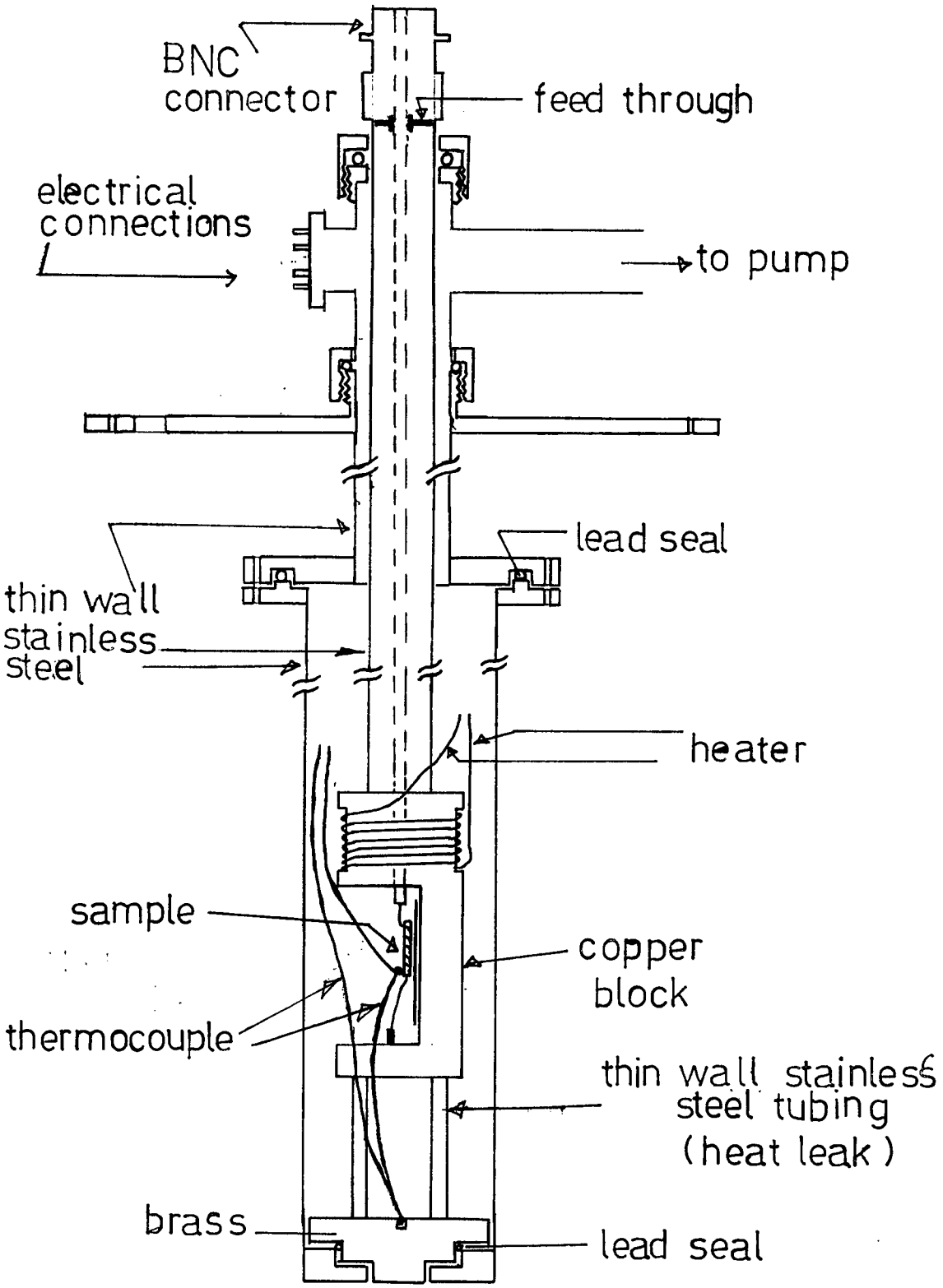

Fig.(15): Low temperature cryostat and crystal holder

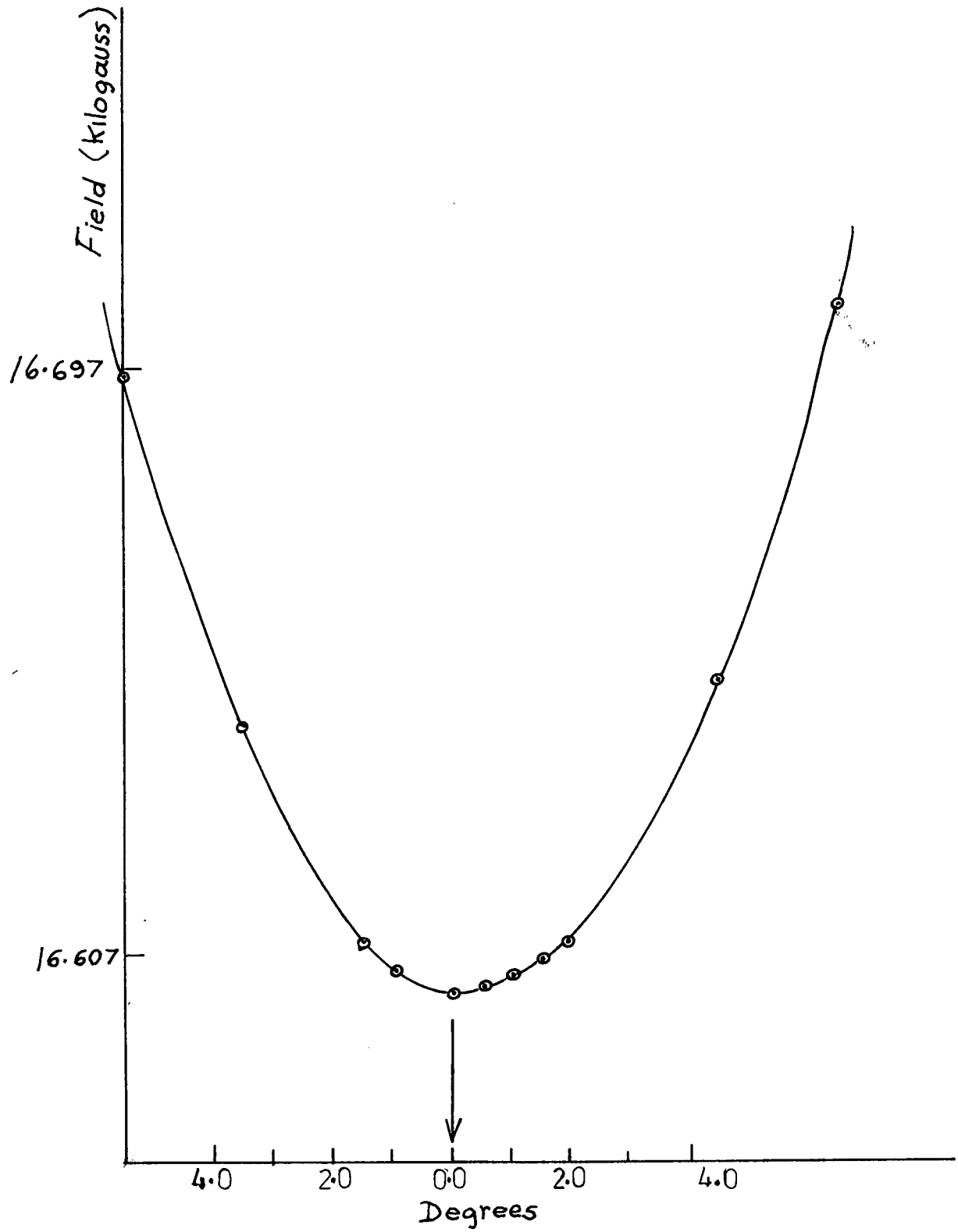

Fig. (16): Angular dependance of the $|9/2, 1/2\rangle \rightarrow |9/2, -1/2\rangle$ resonance.

CHAPTER IV

RESULTS

The preliminary data upon the sample was taken by Dr. M.I. Valic. This data showed that the $|\frac{9}{2}, \frac{1}{2}\rangle \rightarrow |\frac{9}{2}, -\frac{1}{2}\rangle$ line observed with the magnetic field parallel to the c axis of the crystal was unchanged as a function of temperature for temperatures above 30K. At lower temperatures the line broadened and a transition was observed near 24K. At still lower temperatures (10K and lower) an additional broad base line feature appeared. In contrast the lines affected by the quadrupole interaction, for example the $|\frac{9}{2}, \frac{1}{2}\rangle \rightarrow |\frac{9}{2}, \frac{3}{2}\rangle$ line, broadened as the temperature was decreased below 40K and were unobservably broad at 24K.

To further study this problem, a new set of data was taken at a higher field and both sets of data were analysed. For the purpose of this thesis we will restrict our analysis to the temperature dependence of the $|\frac{9}{2}, \frac{1}{2}\rangle \rightarrow |\frac{9}{2}, -\frac{1}{2}\rangle$ line and the determination of the quadrupole interaction and the Knight shifts at room temperature and 77K.

Temperature dependence of the $|\frac{9}{2}, \frac{1}{2}\rangle \rightarrow |\frac{9}{2}, -\frac{1}{2}\rangle$ line

Line shapes were obtained at temperatures between 5.2K and 50K for fixed frequencies of 10.443 MHZ, 12.217 MHZ, 15.822 MHZ and 18.000 MHZ. At temperatures below 5.0K the sample was a superconductor. At lower fields the lines broadened as the temperature was lowered below 30K and a transition was observed near 24K. The high field data showed a transition near 18K and no broad base line feature. Figs. 17-22 show the line shape above, near, and below the transition. The variation of the line width as a function of temperature is shown in Fig. 23.

Determination of e^2qQ/h and the Knight Shifts

The quadropole frequency ν_Q and the Knight Shifts $K_{\parallel}$ and $K_{\perp}$ were calculated from the spectra obtained at room temperature and 77K. The

separation between the $|\frac{9}{2}, \frac{1}{2}\rangle \rightarrow |\frac{9}{2}, -\frac{1}{2}\rangle$ and $|\frac{9}{2}, \frac{1}{2}\rangle \rightarrow |\frac{9}{2}, -\frac{3}{2}\rangle$ lines gave a direct measurement of ν_Q. A sample calculation of $K_\perp$ is shown in Fig. 24. The calculated values of $e^2qQ/h = 24\nu_Q$, K_{iso} and K_{aniso} are listed in Table (II) below.

	Room temperature	77 K
$K_{\parallel}$	0.41 ± .04%	0.39 ± .01%
$K_\perp$	-0.12 ± .01%	-0.19 ± .02%
K_{iso}	0.06 ± .02%	0.00 ± .02%
K_{aniso}	0.35 ± .03%	0.39 ± .02%
$\frac{e^2qQ}{h}$	59853.6 ± 60.0 kHz	61864.8 ± 32.0 kHz

Table (II): The quadrupole interaction and the Knight Shifts at room temperature and 77 K.

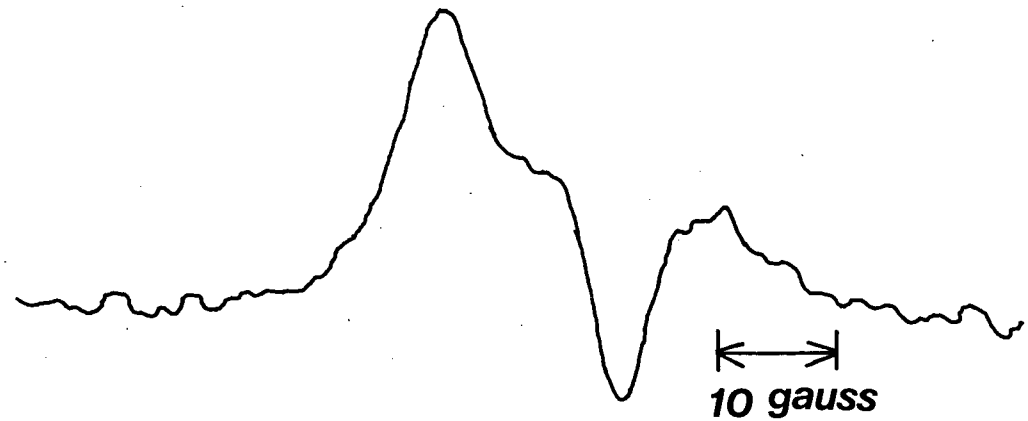

Fig. (17): Nb^{93} in $NbSe_2$ $|9/2, 1/2\rangle \rightarrow |9/2, -1/2\rangle$ line shape at 5.9 K and 12.22 MHz with $\vec{H}$ parallel to $\vec{c}$

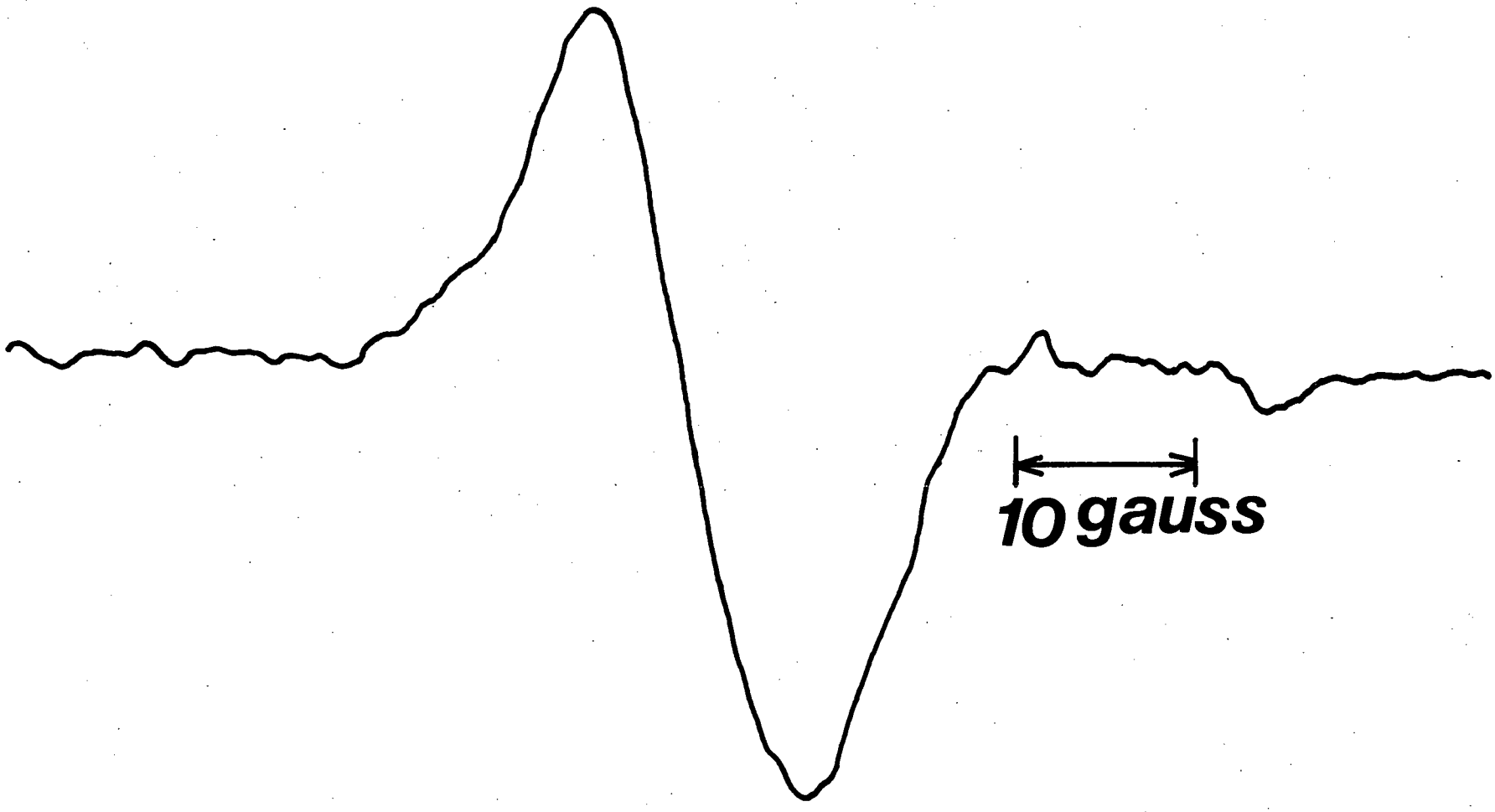

Fig. (18): Nb^{93} in $NbSe_2$ $|9/2, 1/2\rangle \rightarrow |9/2, -1/2\rangle$ line shape at 21.3K and 12.22 MHz with $\vec{H}$ parallel to $\vec{c}$.

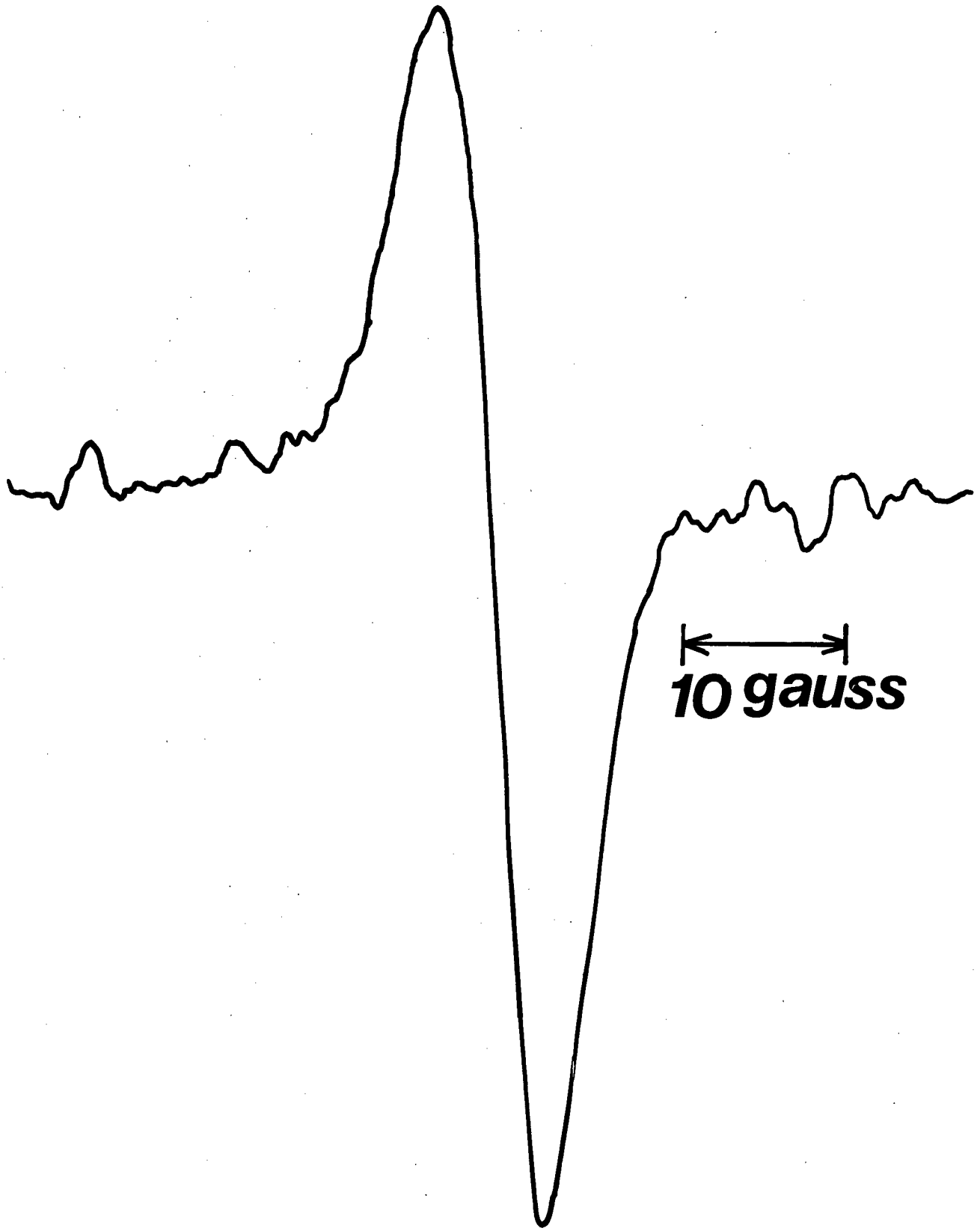

Fig. (19): Nb^{93} in $NbSe_2$ $|9/2, 1/2\rangle \rightarrow |9/2, -1/2\rangle$ line shape at 29 K and 12.22 MHz with $\vec{H}$ parallel to $\vec{c}$.

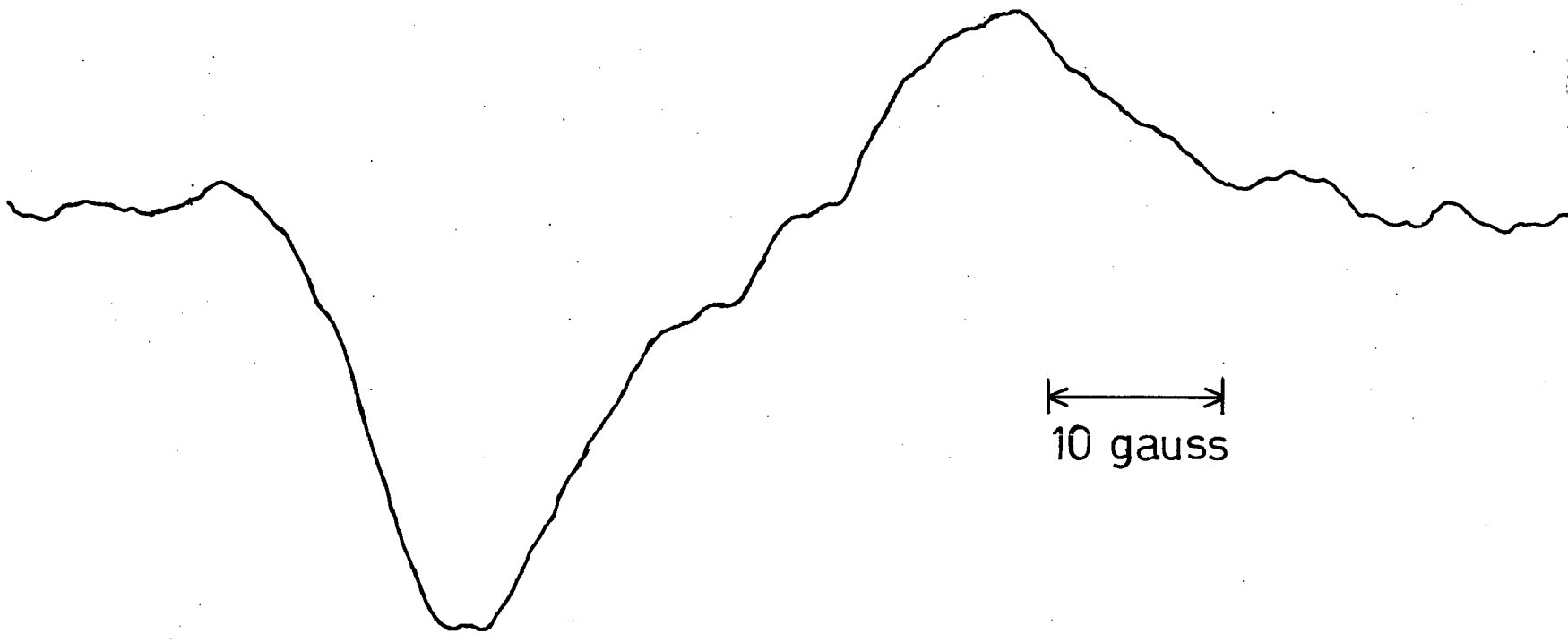

Fig. (20): Nb^{93} in $NbSe_2$ $|9/2, 1/2\rangle \rightarrow |9/2, -1/2\rangle$ line shape at 6.6K and 18.00 MHz with $\vec{H}$ parallel to $\vec{c}$.

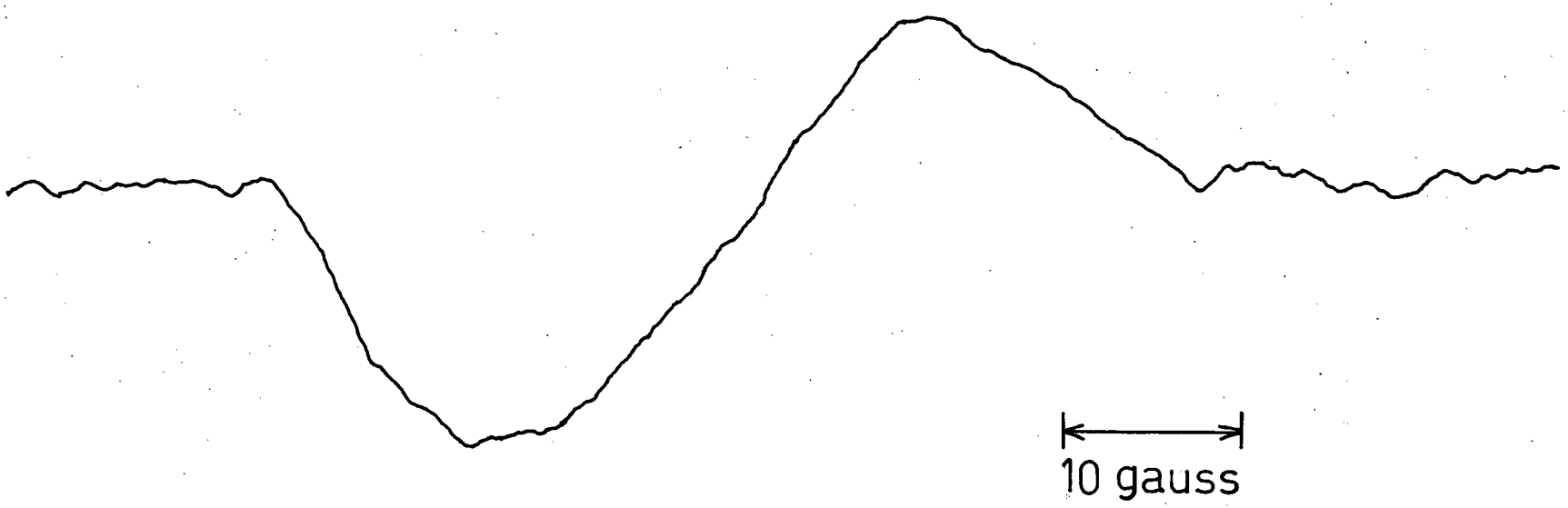

Fig. (21): Nb^{93} in $NbSe_2$ $|9/2, 1/2\rangle \rightarrow |9/2, -1/2\rangle$ line shape at 12.6K and 18.00 MHz with $\vec{H}$ parallel to $\vec{c}$.

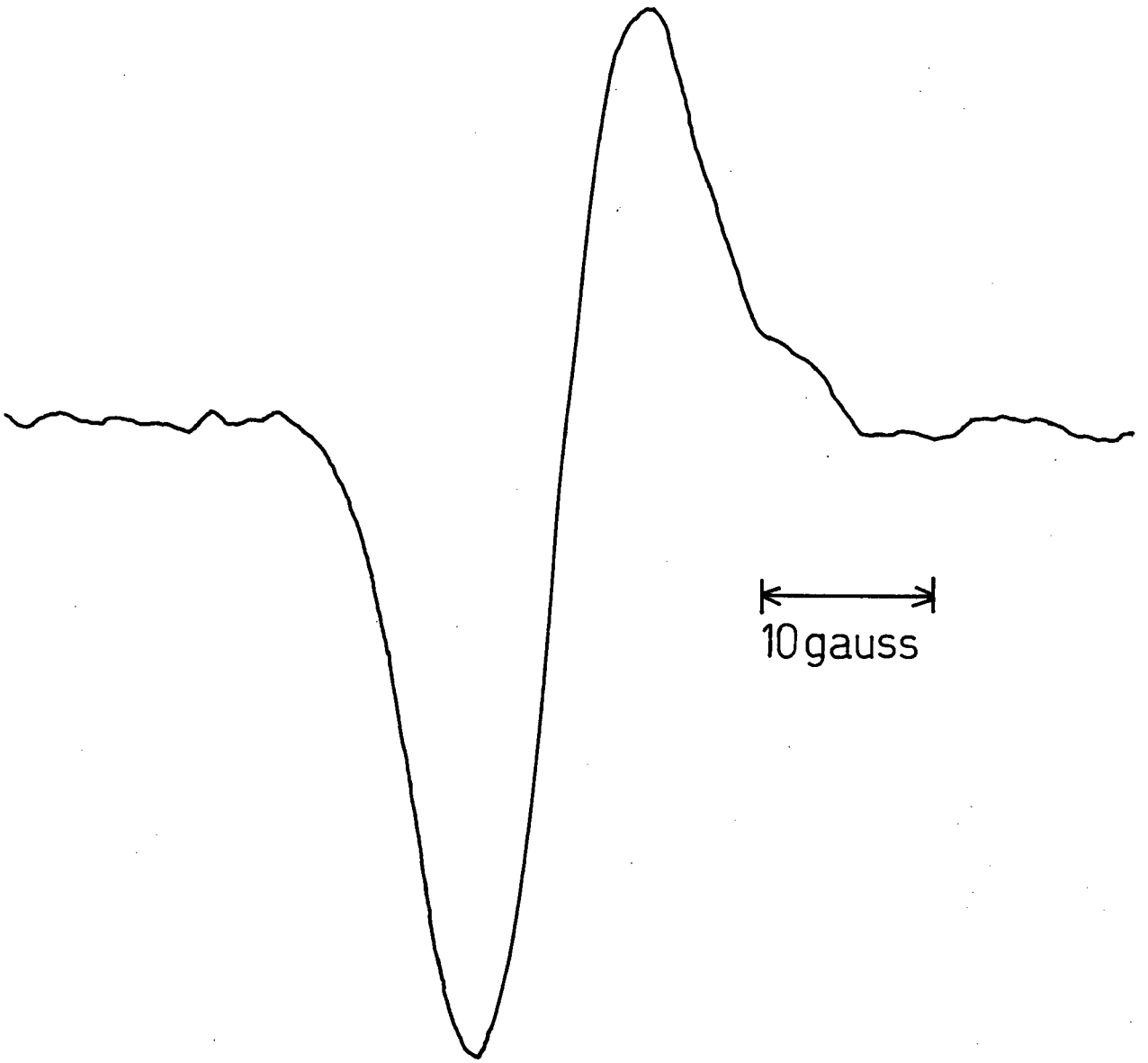

Fig. (22): Nb^{93} in $NbSe_2$ $|9/2, 1/2\rangle \rightarrow |9/2, -1/2\rangle$ line shape at 20.6 K and 18.00 MHz with $\vec{H}$ parallel to $\vec{c}$.

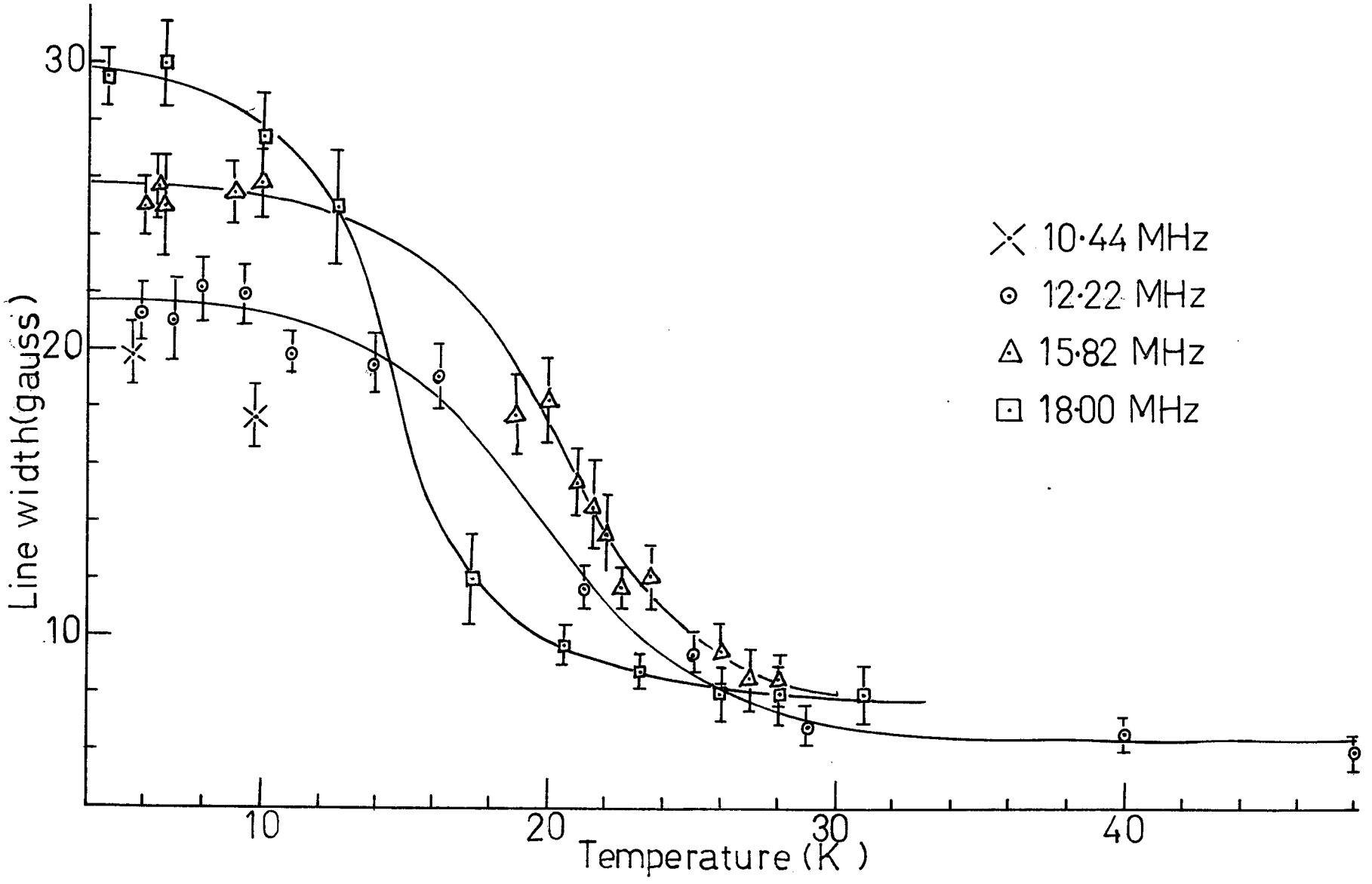

(Fig. 23): Temperature and field dependence of the line width for the $|9/2, 1/2\rangle \rightarrow |9/2, -1/2\rangle$ line with $\vec{H}$ parallel to $\vec{c}$. The line width specified is the peak-to-peak of the derivative spectrum.

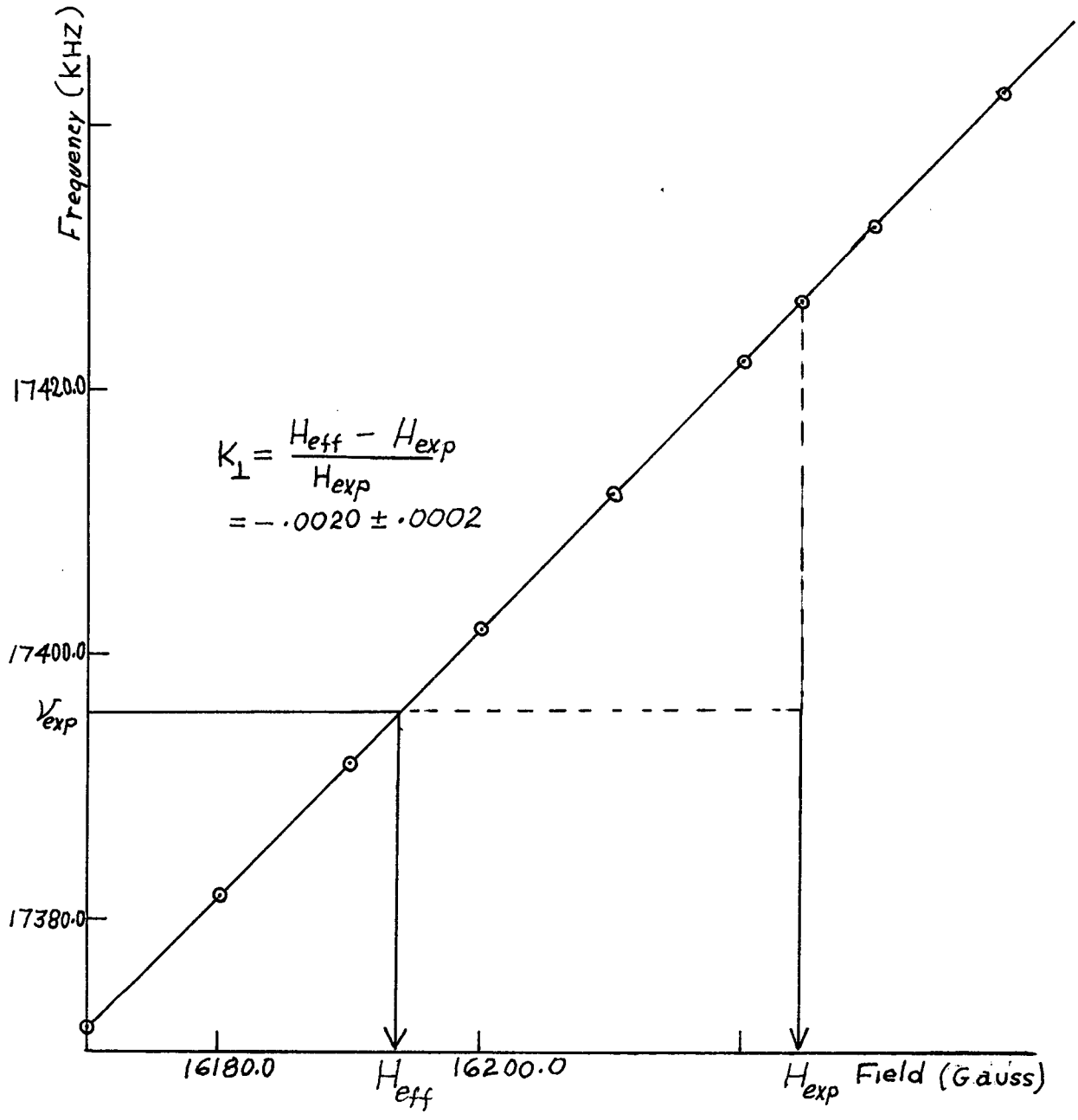

Fig. (24): A sample calculation of $K_\perp$. The calculated resonance frequency $(E_{-1/2} - E_{1/2})/h$ is plotted as a function of applied field. The observed resonance frequency ν_{exp} is due to an effective field H_{eff} at the site of the Nb nucleus which is lower than the applied field H_{exp}.

Discussion

If the transition observed at low temperatures is a result of having two inequivalent Nb sites with different electric field gradients (EFG) as explained by Ehrenfreund and Gossard [2], then it should be possible to fit the line shape obtained at temperatures below the transition with two lines corresponding to the two different sites. This was tried and could not be done.

Moreover, the observed transition could not be due to a low temperature structural distortion alone. Fig.(24) shows the dependence of the calculated frequency of the $|\frac{9}{2}, \frac{1}{2}\rangle \rightarrow |\frac{9}{2}, -\frac{1}{2}\rangle$ line as a function of the asymmetry parameter η. It is clear that η must be much larger than .05, as quoted by Gossard, in order to have any effect compatible with our experimental results. The calculated frequency shift for η = .05 is 0.5 KHZ and is independent of field in the range between 13 and 17.5 KG. The effect of taking η into account is not only negligible but also yields the wrong field dependence.

However if the splitting below the transition is plotted as a function of applied field, as shown in Fig.(26), it can be seen that the zero field splitting is just the line width obtained above the transitions. This indicates that the line shape is not a superposition of just two lines but is a result of a distribution of Knight Shifts. In other words the line shape below the transition is a convolution of some distribution function whose breadth is linear in field, and the line shape function above the transition.

The change in the transition temperature from 24K to 18K at high field is an indication that the NMR properties of the sample are dependent upon its mechanical and thermal history. A preliminary experiment on a specimen with 1% excess Nb showed no transition at all.

Finally we note that the temperature variation of the Knight Shift

and e^2qQ_h between 77K and room temperature is indicative of some change in the electron wavefunctions with temperature. It is particularly interesting that K_{iso} is very small and in fact essentially zero at 77K. This indicates that the S-electron character of the electron wavefunctions at the Fermi surface is very small. In contrast the very large anisotropy of the Knight Shift -- as far as we know, the largest yet observed -- is strong evidence for a large P_Z component in the electron wavefunctions (where Z is parallel to c). This strong directional effect must be related to the structure of the Fermi surface of $NbSe_2$.

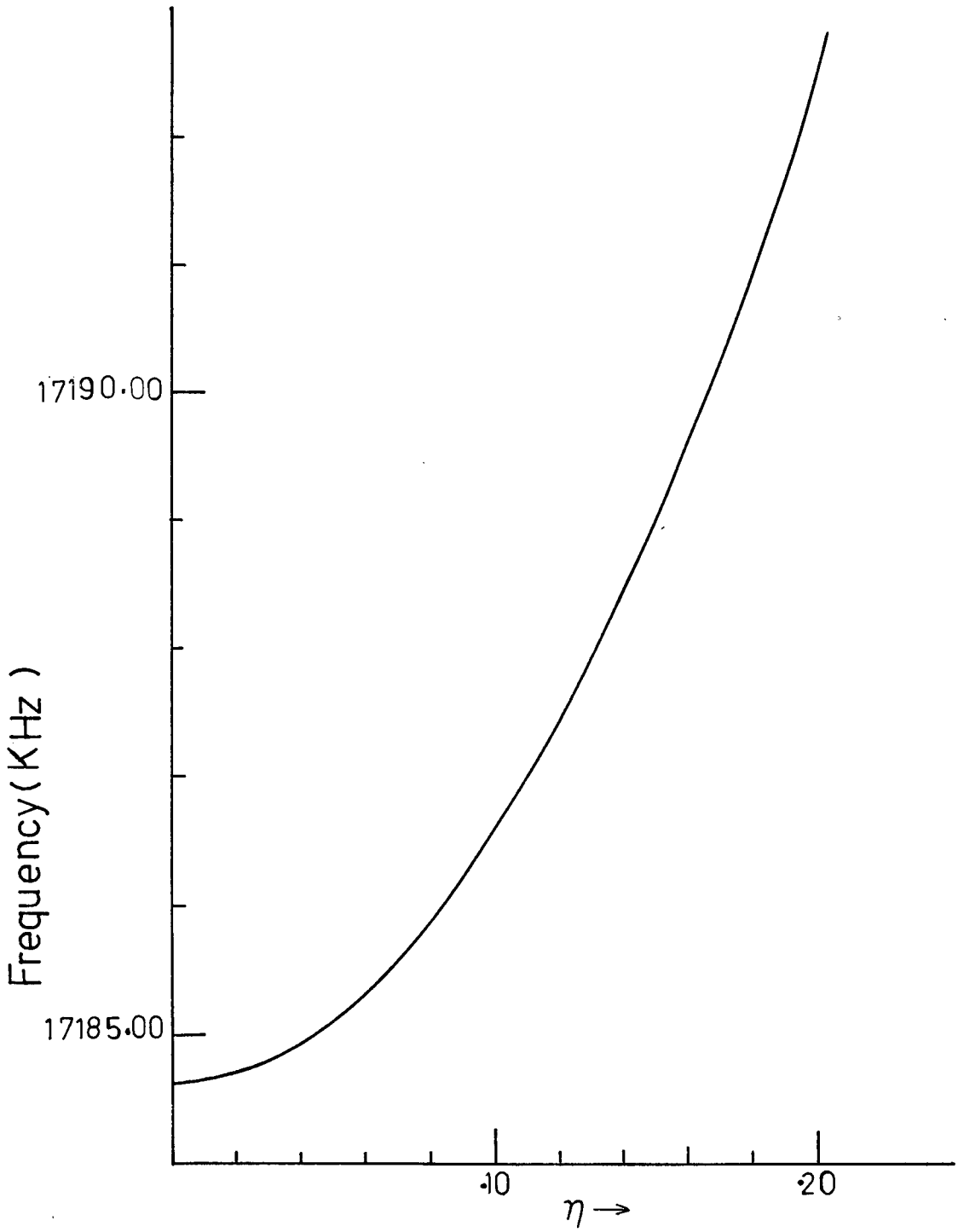

Fig. (25): The variation of the $|9/2, 1/2\rangle \rightarrow |9/2, -1/2\rangle$ frequency as a function of η.

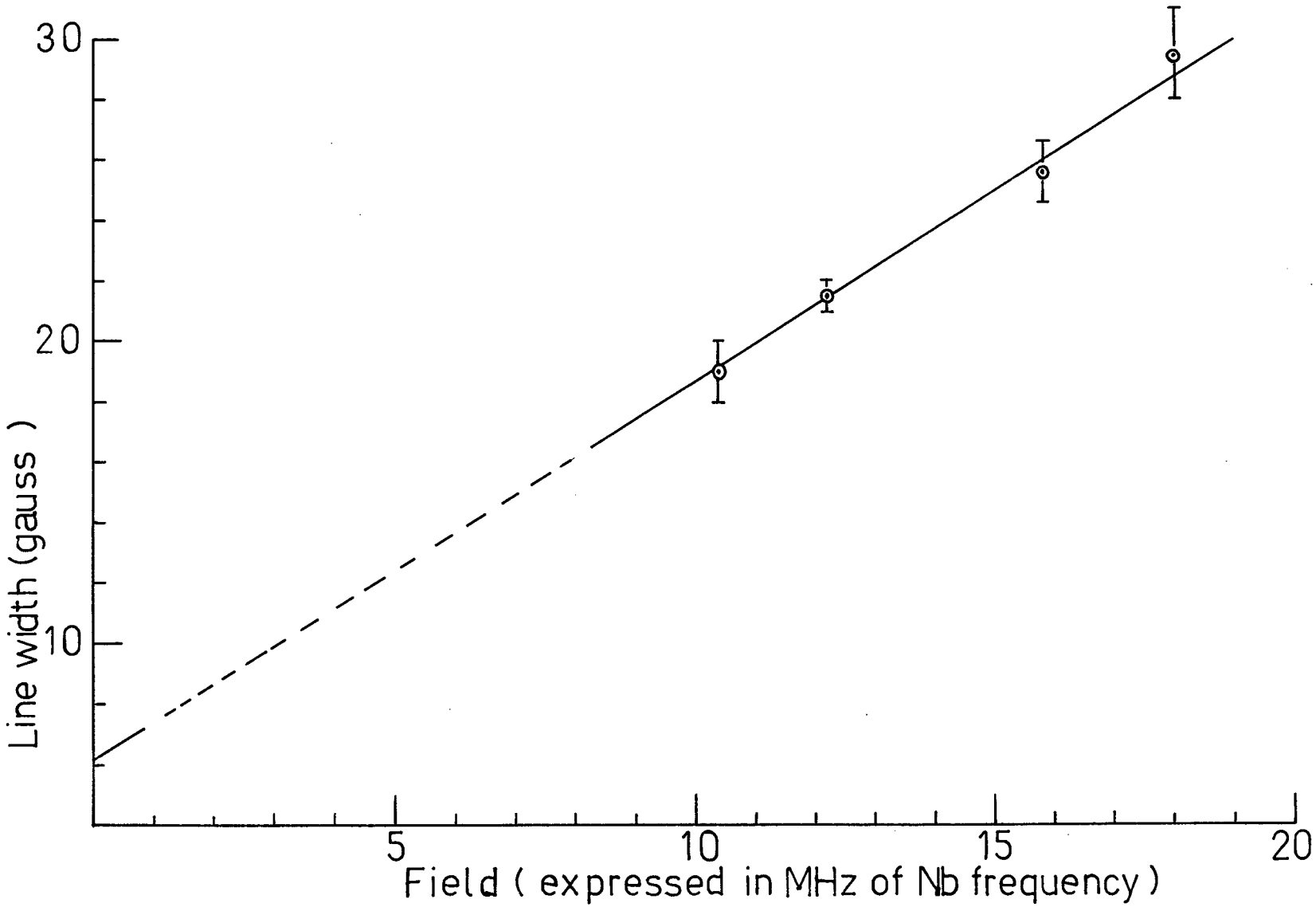

Fig. (26): Field dependence of the line width of the $|9/2, 1/2\rangle \rightarrow |9/2, -1/2\rangle$ line well below the transition.

CONCLUSION

In this thesis we have successfully constructed an FET Robinson spectrometer which we have used in an initial study of $NbSe_2$. The results obtained demonstrate that below a certain transition temperature the Nb nuclei experience a distribution of Knight shifts which implies that some long range feature is associated with the low temperature phase which results in many non-equivalent Nb sites. It is clear that to resolve this feature requires a detailed study of $NbSe_2$ as a function of sample purity, magnetic field, and temperature. In addition the study of the temperature variation of the Knight shift and electric field gradient parameters in the hexagonal phase should give interesting information on the electron wavefunctions. In all of the above, clearly the use of single crystal specimens is essential.

REFERENCES

[1] A. Abragam, The Principles of Nuclear Magnetism. Oxford University Press (1961), p. 200-205.

[2] E. Ehrenfreund, A.C. Gossard, F.R. Gamble and T.H. Gebale, J. of Apl. Phys. 42, 4 (1971).

[3] Walter N. Hardy, unpublished lecture notes, University of British Columbia (1972).

[4] Charles P. Poole, Jr., and Horacio A. Farach, The Theory of Magnetic Resonance. John Wiley and Sons (1972), p.208

[5] F.N.H. Robinson, Journal of Scientific Instruments, Vol. 36 (1959).

[6] T.J. Rowland, Progress in Materials Science, Vol. 9, No. 1 (1961), p.1.

[7] J.A. Wilson and A.D. Yaffe, Advances in Physics 18, 73 (1969).

[8] G.D. Watkins, Thesis, Harvard University.

[9] J. Winter, Magnetic Resonance in Metals. Oxford University Press (1971),

Unlisted references:

[10] M.I. Valic, Thesis, University of British Columbia.

[11] A. Vanderzeil, Noise Sources, Characterization and Measurement. Prentice Hall (1970).

[12] A. Vanderzeil, Noise in Solid State Devices and Lasers, I.E.E.E. Proc., 58, 8 (August, 1970).

[13] Richard S.C. Golbold, Theory and Application of Fets. John Wiley and Sons (1970).

APPENDIX A

Explicit form for the matrix of the Hamiltonians for a spin $\frac{9}{2}$; arbitrary orientation of the magnetic field.

For arbitary θ, ϕ the total Hamiltonian (Zeeman plus quadrupolar) is given, in the notations of Chapter II, by:

$$\underset{\sim}{H} = \frac{h\nu_Q}{6}\left[-\gamma\left\{\frac{\sin\theta\cos\phi}{2}(I_{++} + I_{-}) - \frac{i\sin\theta\sin\psi(I_{+} - I_{-})}{2} + \cos\theta I_{Z}\right.\right.$$

$$\left.\left. + 3I_{Z}^2 - I(I+1) + \frac{\eta}{2}(I_{+}^2 + I_{-}^2)\right]\right.$$

For brevity let

$$\gamma\,\frac{\sin\theta\cos\phi}{2} = \alpha$$

$$\gamma\,\frac{\sin\theta\sin\phi}{2} = \beta$$

$$\gamma\cos\theta = \delta.$$

Then

$$\underset{\sim}{H} = \frac{h\nu_Q}{6}\left[-\alpha(I_{+} + I_{-}) + i\beta(I_{+} - I_{1}) + \frac{\eta}{2}(I_{+}^2 + I_{-}^2)\right]$$

Or in dimensionless units,

$$\frac{6}{h\nu_Q}(\underset{\sim}{H}) = \left[-\alpha(I_{+} + I_{-}) + i\beta(I_{+} - I_{-}) + \frac{\eta}{2}(I_{+}^2 + I_{-}^2)\right].$$

The matrix representative for $\frac{6}{h\nu_Q}(\underset{\sim}{H})$ is given by

$$\frac{6}{h\nu_Q}\underset{\sim}{H} =$$

$36-\frac{9}{2}\delta$	$-3\alpha+3\beta i$	6η							
$-3\alpha-3\beta i$	$12-\frac{7}{2}\delta$	$-4\alpha+4\beta i$	$2\sqrt{21}\,\eta$						
6η	$-4\alpha-4\beta i$	$-6-\frac{5}{2}\delta$	$-\sqrt{21}\alpha+\sqrt{21}\beta i$	$3\sqrt{14}\,\eta$					
	$2\sqrt{21}\,\eta$	$-\sqrt{21}\alpha-\sqrt{21}\beta i$	$-18-\frac{3}{2}\delta$	$-2\sqrt{6}\alpha$ $+2\sqrt{6}\beta i$	$5\sqrt{6}\,\eta$				
		$3\sqrt{14}\,\eta$	$-2\sqrt{6}\alpha$ $-2\sqrt{6}\beta i$	$-24-\frac{1}{2}\delta$	$-5\alpha+5\beta i$	$5\sqrt{6}\,\eta$			
			$5\sqrt{6}\,\eta$	-5α $-5\beta i$	$-24+\frac{1}{2}\delta$	$-2\sqrt{6}\alpha$ $+2\sqrt{6}\beta i$	$3\sqrt{14}\,\eta$		
				$5\sqrt{6}\,\eta$	$-2\sqrt{6}\alpha$ $-2\sqrt{6}\beta i$	$-18+\frac{3}{2}\delta$	$-\sqrt{21}\alpha$ $+\sqrt{21}\beta i$	$2\sqrt{21}\,\eta$	
					$3\sqrt{14}\,\eta$	$-\sqrt{21}\alpha$ $-\sqrt{21}\beta i$	$-6+\frac{5}{2}\delta$	-4α $+4\beta i$	6η
						$2\sqrt{21}\,\eta$	-4α $-4\beta i$	$12+\frac{7}{2}\delta$	-3α $+3\beta i$
							6η	-3α $-3\beta i$	$36+\frac{9}{2}\delta$

APPENDIX B

```
C     A COMPUTER PROGRAMME FOR DIAGONALIZING THE TOTAL
C     HAMILTONIAN(ZEEMAN+QUADRUPOLAR) FOR A SPIN 9/2 FOR AN
C     ARBITRARY ORIENTATION OF THE MAGNETIC FIELD.
C     IT CALCULATES THE EXACT EIGENVALUES AND THE CORRESPONDING
C     NORMALIZED EIGENVECTORS.
C              THE INPUT PARAMETRS ARE:
C     BZERO=APPLIED MAGNATIC FIELD
C     ZMUQ=THE QUDRUPOLE FREQUENCY
C     THETA,PHI SPECIFY  THE ORIENTATION OF THE MAGNETIC FIELD
C     WITH RESPECT TO THE PRINCPAL AXES OF THE ELECTRIC FIELD
C     GRADIENT TENSOR.
C     ETA=ASYMMETRY PARAMETER.


      IMPLICIT REAL*8(A-H,O-Z)
      REAL*8DSQRT
      DIMENSION AR(10,10),AI(10,10),ER(10),EI(10),VR(10,10),VI(10,10)
10    READ(5,2,END=999)BZERO,ZMUQ,THETA,PHI,ETA
      PRINT 503,BZERO,ZMUQ,THETA,PHI,ETA
503   FORMAT('1',5X,T15,'BZERO',T30,'ZMUQ',T50,'THETA',
     1T69,'PHI',T89,'ETA'//6X,2F15.3,3F20.6//)
      XMUL=1.0407D0*BZERO
      Y=6.D0*XMUL/ZMUQ
      WRITE(6,19)Y
19    FORMAT(/,'   Y=',F15.5)
      ALFA=Y*DSIN(THETA)*DCOS(PHI)/2.D0
      BETA=Y*DSIN(THETA)*DSIN(PHI)/2.D0
      DELTA=Y*DCOS(THETA)
2     FORMAT(5F15.6)
      DO 3 J=1,10
      DO 3 I=1,10
      AR(I,J)=0.D0
3     AI(I,J)=0.D0
      AR(1,1)=36.D0-4.5D0*DELTA
      AR(2,2)=12.D0-3.5D0*DELTA
      AR(3,3)=-6.D0-2.5D0*DELTA
      AR(4,4)=-18.D0-1.5D0*DELTA
      AR(5,5)=-24.D0-0.5D0*DELTA
      AR(6,6)=-24.D0+0.5D0*DELTA
      AR(7,7)=-18.D0+1.5D0*DELTA
      AR(8,8)=-6.D0+2.5D0*DELTA
      AR(9,9)=12.D0+3.5D0*DELTA
      AR(10,10)=36.D0+4.5D0*DELTA
      AR(1,2)=-3.D0*ALFA
      AI(1,2)=3.D0*BETA
      AR(2,3)=-4.D0*ALFA
      AI(2,3)=4.D0*BETA
      AR(3,4)=-DSQRT(21.D0)*ALFA
      AI(3,4)=DSQRT(21.D0)*BETA
      AR(4,5)=-2.D0*DSQRT(6.D0)*ALFA
```

```
      AI(4,5)=2.D0*DSQRT(6.D0)*BETA
      AR(5,6)=-5.D0*ALFA
      AI(5,6)=5.D0*BETA
      AR(6,7)=-2.D0*DSQRT(6.D0)*ALFA
      AI(6,7)=2.D0*DSQRT(6.D0)*BETA
      AR(7,8)=-DSQRT(21.D0)*ALFA
      AI(7,8)=DSQRT(21.D0)*BETA
      AR(8,9)=-4.D0*ALFA
      AI(8,9)=4.D0*BETA
      AR(9,10)=-3.D0*ALFA
      AI(9,10)=3.D0*BETA
      DO 100 M=1,9
      DO 100 N=2,10
      AR(N,M)=AR(M,N)
100   AI(N,M)=-1.D0*AI(M,N)
      AR(1,3)=6.D0*ETA
      AR(2,4)=2.D0*DSQRT(21.D0)*ETA
      AR(3,5)=3.D0*DSQRT(14.D0)*ETA
      AR(4,6)=5.D0*DSQRT(6.D0)*ETA
      AR(5,7)=5.D0*DSQRT(6.D0)*ETA
      AR(6,8)=3.D0*DSQRT(14.D0)*ETA
      AR(7,9)=2.D0*DSQRT(21.D0)*ETA
      AR(8,10)=6.D0*ETA
      DO 200 MM=1,8
      DO 200 NN=3,10
200   AR(NN,MM)=AR(MM,NN)
      CALL DCEIGN(AR,AI,10,10,ER,EI,VR,VI,IERROR,1,0)
      N1=10
      IF (IERROR.GT.0) GO TO 20
      DO 500 IROW=1,10
      SUM=0.D0
      DO 501 ICOL=1,10
501   SUM=SUM+VR(IROW,ICOL)**2 +VI(IROW,ICOL)**2
      SUM=DSQRT(SUM)
      DO 502 ICOL=1,10
      VR(IROW,ICOL)=VR(IROW,ICOL)/SUM
502   VI(IROW,ICOL)=VI(IROW,ICOL)/SUM
500   CONTINUE
      PRINT 4
4     FORMAT('0',T5,'EIGENVALUES',T50,'EIGENVECTORS'//)
      DO 5 I=1,10
5     PRINT 6,ER(I),(VR(I,J),J=1,10)
6     FORMAT('0',F11.5,1X,10F9.5)
20    N1=IERROR-1
      DO 8 KK=1,10
      DO 8 KKK=1,10
      AR(KK,KKK)=0.D0
8     AI(KK,KKK)=0.D0
      DO 9 KJ=1,10
9     ER(KJ)=0.D0
      GO TO 10
999   PRINT 11
11    FORMAT('1')
      STOP
      END
```